Studies of the linear energy transfer and relative biological effectiveness in proton therapy of pediatric brain tumors

Lars Fredrik Fjæra

Thesis for the degree of Philosophiae Doctor (PhD)
University of Bergen, Norway
2021

UNIVERSITY OF BERGEN

Studies of the linear energy transfer and relative biological effectiveness in proton therapy of pediatric brain tumors

Lars Fredrik Fjæra

Thesis for the degree of Philosophiae Doctor (PhD)
at the University of Bergen

Date of defense: 25.11.2021

Year: 2021

Title: Studies of the linear energy transfer and relative biological effectiveness in proton therapy of pediatric brain tumors

Name: Lars Fredrik Fjæra

Print: Skipnes Kommunikasjon / University of Bergen

Supervisors

Kristian Smeland Ytre-Hauge

Department of Physics and Technology, University of Bergen, Norway

Camilla Hanquist Stokkevåg

Department of Oncology and Medical Physics, Haukeland University Hospital, Norway

Department of Physics and Technology, University of Bergen, Norway

Ludvig Paul Muren

Department of Medical Physics, Aarhus University Hospital, Denmark

Olav Dahl

Department of Oncology and Medical Physics, Haukeland University Hospital, Norway

Scientific environment

This PhD study has been a part of the project *3D microdosimetry and studies of the Relative Biological Effectiveness (RBE) in proton and carbon ion therapy* funded by the University of Bergen and Trond Mohn Foundation. The project has been organized by Associate Professor Kristian Smeland Ytre-Hauge, within the subatomic physics group at Department of Physics and Technology at the University of Bergen where most of the work in this thesis was conducted.

This study has been in collaboration with physicists, medical doctors and treatment planners from the Haukeland University Hospital as well as the Aarhus University and Aarhus University Hospital.

The projects in this study have also been conducted in close collaboration with the University of Florida Health Proton Therapy Institute (UFHPTI) in Jacksonville, Florida, USA. Between 2017 and 2018 a total of three months were spent at the institute.

Acknowledgements

First and foremost, I want to express my gratitude to my main supervisor, Kristian Smeland Ytre-Hauge. Thank you for being supportive, encouraging, and helpful. Thank you for always keeping your door open and for continuously providing invaluable feedback during my PhD.

I would also like to thank Camilla Hanquist Stokkevåg for your endless enthusiastic spirit and passion. When I doubted my results, you were always there to provide vital guidance.

Thanks to Ludvig Muren for always showing interest in my projects and for always taking the time to review my work.

I want to acknowledge Olav Dahl and Yasmin Lassen-Ramshad for both sharing your time and clinical expertise.

I am very grateful for having had the privilege to work with some of the greatest experts on proton therapy at the University of Florida Health Proton Therapy Institute. A special thanks to Danny Indelicato for your endless encouragement, enthusiasm, and clinical insight.

I want to express my deepest gratitude to all co-authors that have assisted in this project.

Thank you to all collaborators at the Department of Oncology and Medical Physics at Haukeland and in particular thanks to Anfinn Mehus for all the support I have received.

A large thanks to all my friends and colleagues at IFT. Thanks to Eivind and Helge for all help and rewarding discussions, and especially to Tordis for all your assistance, in particular during finalization of the thesis.

A warm thank you to mom and dad for your unconditional love and support, and to the rest of my family and friends for all encouragement and joyful moments outside of work.

Last, but not least, Linn. Thank you for being so patient with me these years, often spending long hours at the office. You have always been there when I needed someone to speak with. Your constant love, support, and kindness have meant a lot.

Abstract

Proton therapy offers a reduction in dose to normal tissue compared to conventional photon-based radiotherapy. This is of particular benefit for pediatric patients as the majority are expected to become long-term survivors. Children are therefore often referred to proton therapy in order to reduce the risk of radiation induced side effects. Protons are also slightly more biologically effective compared to photons, quantified by the clinically applied relative biological effectiveness (RBE) of 1.1. However, both experimental and clinical data points to a variable RBE, which depends on tissue type, dose level, biological endpoint, and the linear energy transfer (LET). Multiple variable RBE models have therefore been developed with the aim of quantifying the RBE variation.

Brain tumor patients are often at high risk of radiation damage to the brainstem - a vital organ where injury can lead to devastating side effects. Minimizing doses to the brainstem has therefore a high priority during treatment planning. However, the brainstem may also be adversely affected by the LET and variable RBE, factors that are not explicitly accounted for in routine proton therapy. In this PhD project, for both double scattering and intensity modulated proton therapy (IMPT), the LET and variable RBE in the brainstem for pediatric brain tumor patients were studied using the FLUKA Monte Carlo (MC) code.

In the first part of this project, the LET and RBE in the brainstem were studied for different tumor locations relative to the brainstem. Furthermore, techniques for reducing the LET in critical organs by changing the treatment field setup were explored (Paper I). Mean LET values in the brainstem more than doubled depending on the tumor location (3.2-6.6 keV/μm), however, the location with the highest brainstem LET values also had the lowest variable RBE-weighted mean dose in the brainstem (1.8-54.0 Gy(RBE)). Changing treatment field angles reduced the mean LET in the brainstem by 32%, however, with slightly increased brainstem dose. The results demonstrate that the LET and variable RBE-weighted dose are strongly influenced by tumor location and field configuration, and that both LET

and variable RBE-weighted dose must be carefully considered when altering treatment plans.

In the second part, multiple variable RBE models in treatment for pediatric brain tumors were investigated. The spatial agreement of isodose volumes from the models relative to the RBE of 1.1 were compared, focusing on the full brainstem and brainstem substructures (Paper II). Application of different model specific parameters were also explored. The RBE-weighted dose calculated from RBE models was highly dependent on the applied parameters, and also differed across models. Furthermore, the spatial agreement between different models decreased rapidly for higher doses, illustrating that the RBE effect is most critical at high doses and low volumes, where dose constraints commonly are applied. Hence, using RBE models in clinical settings requires model specific dose constraints.

The majority of follow-up data from proton therapy come from patients treated with double scattering (DS) proton therapy. Therefore, a DS nozzle was implemented in the FLUKA MC code in order to obtain LET and variable RBE for previously treated patients (Paper III). After calibration, excellent agreement between measurements and MC simulations was achieved with range differences of spread-out Bragg peaks generally below 1 mm and lateral penumbra differences less than 1 mm. Recalculation of dose distributions in FLUKA were compared to original patient doses from the treatment planning system, with dose differences below 2%. LET and variable RBE were furthermore obtained for these patients.

In the final part of this project, the DS nozzle implementation was used to recalculate 36 pediatric brain tumor patients in a retrospective case-control study where nine patients had experienced symptomatic brainstem toxicity. Differences in LET and variable RBE-weighted dose between cases and controls were examined for the full brainstem as well as multiple brainstem substructures. Median and maximum LET were on average higher for cases vs. controls for all substructures, with the highest difference in median LET of 15% in one of the substructures. Average differences between cases and controls increased for variable RBE-weighted doses compared to a fixed RBE of 1.1. While there was large interpatient variability for both LET and

variable RBE-weighted doses, the average higher LET to the brainstem could be a contributor to brainstem toxicity. The results warrant individual assessment of LET/RBE for patients at risk of brainstem toxicity.

Overall, this thesis has shown that elevated LET and increased RBE may occur in the brainstem for pediatric patients with brain tumors which could further contribute to brainstem toxicity. Clinical implementation of LET and variable RBE-weighted dose calculation is therefore well justified.

List of publications

PAPER I **Fjæra, L F**, Li, Z, Ytre-Hauge, K S, Muren, L P, Indelicato, D J, Lassen-Ramshad, Y, Engeseth, G M, Brydøy, M, Mairani, A, Flampouri, S, Dahl, O, & Stokkevåg, C H. (2017). Linear energy transfer distributions in the brainstem depending on tumour location in intensity-modulated proton therapy of paediatric cancer. *Acta Oncol*, *56*(6), 763-768. https://doi.org/10.1080/0284186X.2017.1314007

PAPER II **Fjæra, L F**, Indelicato, D J, Ytre-Hauge, K S, Muren, L P, Lassen-Ramshad, Y, Toussaint, L, Dahl, O, & Stokkevåg, C H. (2021). Spatial agreement of brainstem dose distributions depending on biological model in proton therapy of pediatric brain tumors. *Adv Radiat Oncol*, 6(1), 100551. https://doi.org/10.1016/j.adro.2020.08.008

PAPER III **Fjæra, L F**, Indelicato, D J, Stokkevåg, C H, Muren, L P, Hsi, W C, & Ytre-Hauge, K S. (2020). Implementation of a double scattering nozzle for Monte Carlo recalculation of proton plans with variable relative biological effectiveness. *Phys Med Biol*, 65(22), 225033. https://doi.org/10.1088/1361-6560/abc12d

PAPER IV **Fjæra, L F**, Indelicato, D J, Ytre-Hauge, K S, Lassen-Ramshad, Y, Handeland, A H, Muren, L P, & Stokkevåg C H. Regional difference in relative biological effectiveness and pediatric brainstem toxicity. *Manuscript in preparation.*

Conference contributions

Oral presentations

- **Fjæra, L F**, Indelicato, D J, Ytre-Hauge, K S, Li, Z, Muren, L P, Lassen-Ramshad, Y, Toussaint, L, Flampouri, S, Dahl, O, & Stokkevåg, C H. (2018). Biological dose to brainstem substructures in scanning proton therapy of paediatric brain tumours. *MedFys 2018*, Kvitfjell, Norway.
- **Fjæra, L F**, Indelicato, D J, Ytre-Hauge, K S, Li, Z, Muren, L P, Lassen-Ramshad, Y, Flampouri, S, Dahl, O, & Stokkevåg, C H. (2017). A spatial analysis of biological dose distributions in the brainstem and its substructures in proton therapy of paediatric brain tumours. *ENLIGHT 2017*, Aarhus, Denmark.
- **Fjæra, L F**, Li, Z, Ytre-Hauge, K S, Muren, L P, Indelicato, D J, Lassen-Ramshad, Y, Engeseth, G M, Brydøy, M, Mairani, A, Flampouri, S, Dahl, O, & Stokkevåg, C H. (2017). Brainstem linear energy transfer in intensity-modulated proton therapy of paediatric brain tumours. *ESTRO 36*, Vienna, Austria.
- **Fjæra, L F**, Li, Z, Ytre-Hauge, K S, Muren, L P, Indelicato, D J, Lassen-Ramshad, Y, Engeseth, G M, Brydøy, M, Mairani, A, Flampouri, S, Dahl, O, & Stokkevåg, C H. (2017). Linear energy transfer within the brainstem in intensity-modulated proton therapy of paediatric brain tumours. *NACP 2017*, Oslo, Norway.

Posters

- **Fjæra, L F**, Indelicato, D J, Ytre-Hauge, K S, Li, Z, Muren, L P, Lassen-Ramshad, Y, Toussaint, L, Flampouri, S, Dahl, O, & Stokkevåg, C H. (2018). Biological dose to brainstem substructures in scanning proton therapy of paediatric brain tumours. *ESTRO 37*, Barcelona, Spain.
- **Fjæra, L F**, Indelicato, D J, Ytre-Hauge, K S, Li, Z, Muren, L P, Lassen-Ramshad, Y, Flampouri, S, Dahl, O, & Stokkevåg, C H. (2017). A spatial analysis of biological dose distributions in the brainstem and its substructures in proton therapy of paediatric brain tumours. *ENLIGHT 2017*, Aarhus, Denmark.
- **Fjæra, L F**, Indelicato, D J, Stokkevåg, C H, Muren, L P, Hsi, W C, & Ytre-Hauge, K S (2020). Implementation of a double scattering nozzle for Monte Carlo recalculation of proton plans with variable relative biological effectiveness. *NACP 2021*, Reykjavik, Iceland (online conference).

Publication contributions

- Dahle, T J, Rykkelid, A M, Stokkevåg, C H, Mairani, A, Görgen, A, Edin, N J, Rørvik, E, **Fjæra, L F**, Malinen, E, & Ytre-Hauge, K S. (2017). Monte Carlo simulations of a low energy proton beamline for radiobiological experiments. *Acta Oncol, 56*(6), 779–786. https://doi.org/10.1080/0284186X.2017.1289239
- Rørvik, E, Thörnqvist, S, Stokkevåg, C H, Dahle, T J, **Fjæra, L F**, & Ytre-Hauge, K S. (2017). A phenomenological biological dose model for proton therapy based on linear energy transfer spectra. *Med Phys, 44*(6), 2586–2594. https://doi.org/10.1002/mp.12216
- Rørvik, E, **Fjæra, L F**, Dahle, T J, Dale, J E, Engeseth, G M, Stokkevåg, C H, Thörnqvist, S, & Ytre-Hauge, K S. (2018). Exploration and application of phenomenological RBE models for proton therapy. *Phys Med Biol, 63*(18), 185013. https://doi.org/10.1088/1361-6560/aad9db
- Ytre-Hauge, K S, **Fjæra, L F**, Rørvik, E, Dahle, T J, Dale, J E, Pilskog, S, & Stokkevåg, C H. (2020). Inter-patient variations in relative biological effectiveness for cranio-spinal irradiation with protons. *Sci Rep, 10*(1), 6212. https://doi.org/10.1038/s41598-020-63164-8
- Dahle, T J, Rusten, E, Stokkevåg, C H, Silvoniemi, A, Mairani, A, **Fjæra, L F**, Rørvik, E, Henjum, H, Wright, P, Boer, C G, Forsback, S, Minn, H, Malinen, E, & Ytre-Hauge, K S. (2020). The FLUKA Monte Carlo code coupled with an OER model for biologically weighted dose calculations in proton therapy of hypoxic tumors. *Phys Med, 76*, 166–172. https://doi.org/10.1016/j.ejmp.2020.07.003

- Otterlei, O M, Indelicato, D J, Toussaint, L, Ytre-Hauge, K S, Pilskog, S, **Fjæra, L F**, Rørvik, E, Pettersen, H E S, Muren, L P, Lassen-Ramshad, Y, Di Pinto, M, & Stokkevåg, C H. (2020). Variation in relative biological effectiveness for cognitive structures in proton therapy of pediatric brain tumors. *Acta Oncol*, 60(2), 267-274. https://doi.org/10.1080/0284186X.2020.1840626
- Henjum, H, Dahle, T J, **Fjæra, L F**, Rørvik, E, Pilskog, S, Stokkevåg, C H, Mairani, A, & Ytre-Hauge, K S. Implementation and exploration of LET and RBE based biological dose optimization in proton therapy. Submitted to Advances in Radiation Oncology

Abbreviations

BCM	Beam current modulation
CT	Computed tomography
CTV	Clinical target volume
dX%	Distal X% (X is the dose level)
DICOM	Digital Imaging and Communications in Medicine
DS	Double scattering
DSB	Double-strand break
DSC	Dice similarity coefficient
DVH	Dose volume histogram
FLAIR	FLUKA Advanced Interface
FLUKA	Fluktuierende Kaskade
GTV	Gross tumor volume
HU	Hounsfield unit
ICRU	International Commission on Radiation Units and Measurements
IMPT	Intensity modulated proton therapy
kV	Kilovoltage
LET	Linear energy transfer
LET$_\mathrm{d}$	Dose-averaged linear energy transfer
LET$_\mathrm{t}$	Track-averaged linear energy transfer
LQ	Linear quadratic
MC	Monte Carlo
MCS	Multiple Coulomb scattering
MRI	Magnetic resonance imaging
MV	Megavoltage
OAR	Organ at risk
pX%	Proximal X% (X is the dose level)

PBS	Pencil beam scanning
PDF	Probability density function
PET	Positron emission tomography
PS	Passive scattering
PRV	Planning organ at risk volume
PTV	Planning target volume
RBE	Relative biological effectiveness
$RBE_{1.1}$	Relative biological effectiveness = 1.1
RM	Range modulator
SOBP	Spread-out Bragg peak
SSB	Single-strand break
TPS	Treatment planning system
UFHPTI	University of Florida Health Proton Therapy Institute

Contents

Scientific environment ii

Acknowledgements iii

Abstract iv

List of publications vii

Conference contributions viii

Publication contributions x

Abbreviations xii

Contents xiv

1 Introduction 1

2 Radiation physics 5

2.1 Proton beam interactions 5
2.2 Linear energy transfer 10
2.3 Proton beam parameters 12

3 Radiobiology 15

3.1 The linear quadratic model 16
3.2 Relative biological effectiveness 17
3.3 Variable RBE in a clinical setting 25

4 Treatment planning and delivery techniques 27

4.1 Treatment planning 27
4.2 Delivery techniques 30
4.3 Monte Carlo simulations 36

5 Pediatric brain tumor patients 39

5.1 The brainstem in proton therapy 39

6 Thesis objective 43

7 Materials and methods 45

7.1 Patient material and calculation software 45
7.2 Recalculation of IMPT plans 45
7.3 Recalculation of DS plans 50
7.4 Ethical considerations 54

8 Summary of results 55

8.1 Paper I: LET variation depending on tumor location 55

8.2 Paper II: Spatial agreement of variable RBE models 56
8.3 Paper III: Implementation of a DS nozzle in a MC system 58
8.4 Paper IV: Variable RBE and pediatric brainstem toxicity 59

9 Discussion 63

9.1 Does the variable proton RBE have a clinical impact on patients? 64
9.2 The need for variable RBE models 66
9.3 Implementing LET and RBE calculation in clinics 69
9.4 Scoring of quantities 70
9.5 Should current clinical practice be revised? 72

10 Conclusions 75

Bibliography 77

Publications 97

1 Introduction

In 2020, an estimated 19.3 million individuals were diagnosed with cancer (The Global Cancer Observatory, 2020). Nearly 10 million people lost their life to the disease, counting for 1 in 6 of all deaths. In developed countries, cancer usually ranks as the first or second leading cause of death for people below the age of 70 (Sung et al., 2021). While cancer has a lot of risk factors, such as tobacco use and radiation exposure, the most prominent factor is age, with an average of 67 years at the diagnosis of cancer (Ruddon, 2007). Nevertheless, children are also at risk of getting cancer, and it is the leading cause of non-accidental death between the ages 1-14. Fortunately, survival rates for childhood cancer have increased rapidly the last 50 years, from 58% in the 1970s to above 80% today (Kassam et al., 2018). With high rates of survival, the second priority is to decrease late effects and morbidity following cancer treatment.

The main modalities of cancer treatment include surgery, chemotherapy, immunotherapy, and radiotherapy. While all modalities have advantages, an estimated 50% of all cancer patients could benefit from radiotherapy (Barton et al., 2014). External radiotherapy is a non-invasive treatment method, intended to kill or control malignant cells, while at the same time sparing healthy tissue. Traced all the way back to 1895 when Wilhelm Röntgen discovered x-rays (Röntgen, 1895), patients have been treated with radiation for almost thirteen decades. During these years, radiotherapy with x-rays has steadily evolved from using photons with kilovoltage (kV) energies delivered by radium tubes to megavoltage (MV) energies using cobalt-

60 machines. Radiotherapy was further revolutionized by the introduction of the linear accelerator in 1948 and later by three-dimensional image acquisition of the patient using computed tomography (CT) and magnetic resonance imaging (MRI) (Thariat et al., 2013). Over the years, new techniques for delivering the radiotherapy were also introduced, such intensity modulated radiotherapy (IMRT) and volumetric modulated arc therapy (VMAT), greatly increasing the dose conformity. All these advancements have continuously improved the delivery precision of radiotherapy.

During the 20th century, radiotherapy using other particles such as protons, neutrons, and electrons has also been explored and used for cancer treatment. The advantages of therapeutic proton therapy compared with conventional photon radiotherapy were first suggested and described by Robert Wilson (1946). The suggestion was based on the finite proton range, the small lateral spread and that the proton ionization per unit length is inversely proportional with the energy. This results in a maximum dose deposition in the last centimeter of the proton range giving rise to the so-called Bragg peak. Hence, in contrast to photons, protons avoid exit doses and greatly reduce the entrance dose, providing an intrinsic increase in dose conformity. Patients have been treated with protons since the 1950s, but the treatment was in the beginning considered experimental and proton therapy was only conducted in research facilities. It was not until the 1990s that the first hospital-based facility was built. Since then, the number of facilities and treated patients have increased rapidly (PTCOG, 2021a, 2021b).

Protons and photons interact with materials based on different physical principles. Protons are more densely ionizing, leading to a slight increase in the biological effect compared to photons - termed the relative biological effectiveness (RBE). The clinically used RBE for protons have been set to 1.1 as recommended by the International Commission on Radiation Units and Measurements (ICRU, 2007), meaning that protons are characterized to be 10% more biological effective compared to photons. While a generic RBE has many advantages, such as simplifying the task of transferring clinical experience and tolerance doses from photon radiotherapy to proton therapy, it is well known that the RBE is not constant. Experiments have shown that the proton RBE is a variable parameter, dependent on quantities such as the tissue type, physical dose, the linear energy transfer (LET), and biological endpoint (Paganetti, 2014).

Of the around 400 000 adolescents that are diagnosed with cancer each year (Steliarova-Foucher et al., 2017), a large portion will receive radiotherapy. Due to their long life expectancy, pediatric patients are at increased risk of experiencing long term morbidity (Oeffinger et al., 2006) and secondary cancers (Bhatia & Sklar, 2002). Pediatric patients are therefore often prioritized to receive proton therapy due to the increased dose conformity of protons. However, as the effect of LET and RBE is currently not quantitatively accounted for in proton therapy clinics, these patients could be adversely affected, either in the form of a lack of tumor control or an increase in damage to healthy tissues and organs at risk (OARs). In fact, retrospective studies have in recent years indicated a correlation between increased RBE and radiation toxicity for patients, including children,

treated with proton therapy (Bahn *et al.*, 2020; Bolsi *et al.*, 2020; Eulitz *et al.*, 2019b; Peeler *et al.*, 2016; Wang *et al.*, 2020; Ödén *et al.*, 2020). These results warrant further investigation.

Monte Carlo (MC) codes are highly versatile tools that can be useful in clinical research regarding radiation treatment. In this PhD project, a general-purpose MC code was used to study the effect of the variable RBE and LET, focusing on pediatric brain tumor patients treated with proton therapy. This also required the implementation and commissioning of a proton therapy treatment nozzle into the MC code.

2 Radiation physics

2.1 Proton beam interactions

Radiotherapeutic protons interact with matter by three distinct processes: stopping by inelastic collisions with atomic electrons, scattering by elastic collisions with atomic nuclei, and non-elastic nuclear interactions. The first two processes are the most common and are well described by theoretical models. The latter does not follow any simple theory but can be treated using correction factors (Gottschalk, 2011). While these interactions occur for all heavy charged particles, the focus will be specifically on proton interactions.

2.1.1 Stopping power

Protons traversing matter will inelastically collide with the much lighter atomic electrons, either exciting or ionizing the electrons. In each interaction, a certain amount of proton energy is transferred to the electrons. Due to the large mass difference between the particles, protons usually lose only a small fraction of the energy per collision. However, these collisions are so frequent that the proton energy continuously decreases, slowing down the proton. Intrinsically, the longer a proton interacts with an electron the more energy it will lose. Thus, slower protons lose more energy, resulting in an increasing energy loss for increasing depth, giving rise to the Bragg peak where the maximum energy loss occurs (Figure 2.1) (Gottschalk, 2011). The Bragg peak is the main advantage of protons over photons in radiotherapy, since by adjusting the proton energy, the Bragg peak can be aimed directly

in the target volume, with only a negligible amount of dose deposited beyond this point.

The energy loss per unit length is termed the stopping power. The stopping power of a projectile of charge, z, and mass, m, in a material of atomic number, Z, and atomic mass, A, can be described by the Bethe Bloch equation (Bethe, 1930; Bloch, 1933a, 1933b):

$$-\frac{dE}{dx} = 4\pi N_A r_e^2 m_e c^2 z^2 \rho \frac{Z}{A}\frac{1}{\beta^2}\left(\frac{1}{2} ln \frac{2m_e c^2 \beta^2 \gamma^2 W_{max}}{I^2} - \beta^2 - \frac{\delta}{2} - \frac{C}{Z}\right), \quad (2.1)$$

where N_A is Avogadro's number, r_e is the classical electron radius, m_e is the electron mass, c is the light speed in vacuum, $\beta = v/c$ where v is the speed of the projectile, γ is the Lorentz factor $(1/\sqrt{1-\beta^2})$, W_{max} is the maximum energy transferrable in a single collision, I is the ionization potential, δ is the density correction and C is the shell correction. Focusing only on protons in the clinical energy range (3-300 MeV), by disregarding the corrections and inserting constants, equation (2.1) can be simplified to (Gottschalk, 2004, 2011):

$$-\frac{dE}{dx} = 0.3072\rho \frac{Z}{A}\frac{1}{\beta^2}\left(ln \frac{W_{max}}{I^2} - \beta^2\right). \quad (2.2)$$

For clinical proton energies, $1/\beta^2$ is the dominant term, illustrating the increase in stopping power for decreasing velocity.

The energy loss of protons is a stochastic process. In a monoenergetic proton beam, protons will interact randomly such that they stop at slightly different depths. This phenomenon is called range straggling, an effect that ultimately widens the pristine Bragg peak in depth. The straggling for protons in water can be approximated by $0.012 \cdot \text{range}$, leading to an increase

in the absolute width of the proton beam for higher ranges (Gottschalk, 2011). Another contributor to the Bragg peak width is the energy spread. The energy spread of a proton beam increases for instance when the beam traverses a medium such as a degrader used for regulating the proton beam energy. The energy spread is dependent on the initial beam energy with lower energies resulting in higher relative energy spreads (Schippers, 2012).

Various definitions can be used to characterize the range of a proton beam. A common definition is the mean projected range classified as the depth of where 50% of the protons stops, not accounting for nuclear interactions (Paganetti, 2012). This corresponds to the depth in water where the distal 80% (d80%) dose of the pristine Bragg peak occurs (Moyers et al., 2007). An advantage of using the mean projected range is that it is independent of the energy spread (Paganetti, 2012).

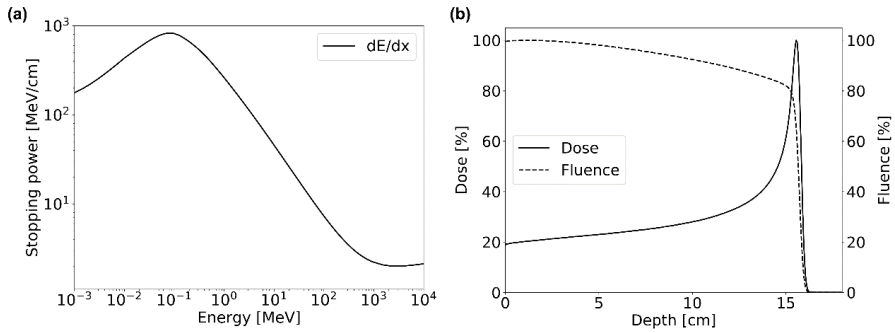

Figure 2.1 a) Stopping power of protons in water as a function of kinetic energy. Figure created using data from Berger et al. (2017). b) 150 MeV monoenergetic proton beam in water. The solid line shows the dose deposit in the form of a pristine Bragg peak. The dashed line shows the fluence of the proton beam. Figure created from Monte Carlo simulations.

2.1.2 Multiple Coulomb scattering

In addition to slowing down through inelastic interactions with electrons, protons also undergo electromagnetic elastic collisions with the atomic nuclei - a process termed multiple Coulomb scattering (MCS). In almost every single collision, the proton is deflected by an almost negligible angle - with rare occurrences of collisions with large scattering angles. As the majority are small-angle deflections, the sum will result in an approximately Gaussian angular distribution. The MCS distributions are well-described by the Moliére theory (Molière, 1947, 1948) which is widely used and has been shown to have an accuracy of within 1% (Gottschalk, 2011). As the theory is quite complex it will not be included here. However, others have developed simpler scattering theories (but of comparable accuracy) such as Highland (1975) who derived his formula by fits to the Moliére theory. The characteristic multiple scattering (CMS) angle for protons can then be calculated using (Highland, 1975):

$$\theta_0 = \frac{14.1\ MeV}{pv}\sqrt{\frac{L}{L_R}}\left[1+\frac{1}{9}\log_{10}\left(\frac{L}{L_R}\right)\right], \tag{2.3}$$

where p and v is the particle momentum and speed, respectively, L is the target thickness while L_R is the so-called radiation length. The radiation length has the following dependency (Patrignani et al., 2016):

$$L_R \propto \frac{A}{Z(Z+1)}, \tag{2.4}$$

where Z and A is the atomic number and the atomic mass, respectively, of the target medium. For a proton with a certain energy, it is evident from the two equations that the CMS angle increases for thicker targets and for

materials of higher atomic numbers, while decreasing for higher beam energies. These dependencies are exploited in passive scattering proton therapy as explained in section 4.2.1. Figure 2.2 shows the difference in MCS for a carbon target ($Z = 6$) and a lead target ($Z = 82$).

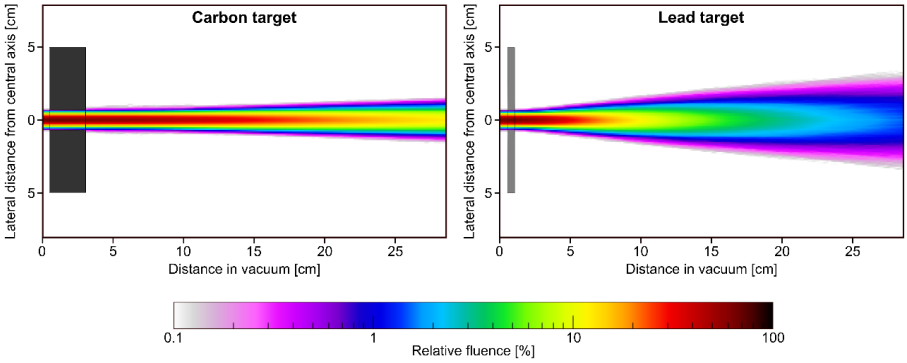

Figure 2.2 Fluence of a 150 MeV proton beam (0.5 cm full-width half maximum) traversing two different targets. Areal densities, $\rho \cdot \Delta x$, have been normalized to illustrate the Z dependence of MCS. Left: 2.5 cm carbon target ($\rho = 2.26\ g/cm^3, Z = 6$). Right: 0.5 cm lead target ($\rho = 11.35\ g/cm^3, Z = 82$). Figures created from Monte Carlo simulations.

2.1.3 Non-elastic nuclear interactions

Non-elastic nuclear interactions occurs when a proton collides with atomic nuclei in a given material and the kinetic energy is not conserved. This is in contrast to MCS, which are elastic nuclear interactions. Non-elastic nuclear interactions can result in excitation of nuclei or nucleus breakup leading to secondaries such as secondary protons, photons, neutrons, heavy particles such as alphas and recoiling residual nucleus. If a so-called primary proton undergoes a non-elastic interaction, it will no longer be characterized as a primary particle but as a secondary particle. This is because it is impossible to tell if the proton is the incident particle or if it originates from the atomic nuclei (Gottschalk, 2011).

For a 160 MeV proton beam in water, approximately 20% of the protons undergo a nuclear interaction (Gottschalk, 2004). The main effect of these interactions is that primary protons are stopped before reaching the Bragg peak, resulting in a few consequences: The dose in the peak region decrease since primary protons are removed from the peak, the dose before the Bragg peak increase as the secondaries have shorter ranges and stop upstream, and an immediate increase in dose also occurs a few centimeters within the material where the interactions reach equilibrium. Furthermore, secondary particles usually have large angles relative to the incoming protons, which can lead to minor dose deposition far from the beam path, in particular for neutral secondaries such as neutrons (Gottschalk, 2011).

2.2 Linear energy transfer

The linear energy transfer (LET) is mean energy lost due to electronic interactions per unit length by an ionizing particle, such as a proton. It is a measure of the ionization density of a particle and is closely related to the stopping power. The LET is defined as (ICRU, 2011):

$$LET = \frac{dE}{dl}, \tag{2.5}$$

where dE is the transferred energy in keV and dl is the length in μm.

When a proton interacts with matter, it will ionize and produce secondary electrons. Many of these electrons will travel a certain distance (away from the incoming particle trajectory) and further ionize the material. Such electrons are termed delta rays. It is therefore often of interest to only look at the energy transferred in vicinity of the incoming particle trajectory, hence a maximum energy transfer, Δ, can be applied. This is called the restricted

LET (LET_Δ) where delta rays with kinetic energies above Δ are excluded. If no Δ is defined, all delta rays are included and the LET is called the unrestricted LET (LET_∞, but most often denoted simply as LET). The LET_∞ is equal to the so-called electronic stopping power, S_{el}, which is the stopping power when only considering the interactions with the atomic electrons of the material (ICRU, 2011).

Along each point in a proton track there will be a variance in the energy transferred per unit length from the protons, giving rise to a spectrum of LET values. However, simplifying the characterization of LET is often preferred, usually accomplished by calculating an average LET in each point. There are two major approaches of averaging the LET; the dose-averaged LET ($\mathrm{LET_d}$), most commonly used in proton therapy, and the track-averaged[1] LET ($\mathrm{LET_t}$). In $\mathrm{LET_t}$, the relative fluence of the ionizing particles is used as a weighting factor. For a location, z, the $\mathrm{LET_t}$ of protons can be calculated by (Guan et al., 2015):

$$LET_t(z) = \frac{\int_0^\infty S_{el}(E)\Phi(E,z)dE}{\int_0^\infty \Phi(E,z)dE} = \frac{\int_0^\infty LET(E)\Phi(E,z)dE}{\int_0^\infty \Phi(E,z)dE}, \tag{2.6}$$

where S_{el} is the electronic stopping power (*i.e.*, the unrestricted LET) for the protons and $\Phi(E,z)$ is the fluence of the protons with kinetic energy E. For the alternative, $\mathrm{LET_d}$, the LET is weighted by the absorbed dose. It is defined as (Guan et al., 2015):

$$LET_d(z) = \frac{\int_0^\infty S_{el}^2(E)\Phi(E,z)dE}{\int_0^\infty S_{el}(E)\Phi(E,z)dE} = \frac{\int_0^\infty LET^2(E)\Phi(E,z)dE}{\int_0^\infty LET(E)\Phi(E,z)dE}. \tag{2.7}$$

[1] Also referred to as fluence-averaged LET or fluence-weighted LET ($\mathrm{LET_f}$).

Since $S_{el}(E)\Phi(E,z)/\rho(z) = D(E,z)$, where $D(E,z)$ is the dose, equation (2.7) becomes:

$$LET_d(z) = \frac{\int_0^\infty LET(E)D(E,z)dE}{\int_0^\infty D(E,z)dE}. \tag{2.8}$$

For a proton beam, both the LET_t and LET_d will be reasonably low (and nearly equal) when entering the material. However, as the as protons traverse and begins to stop, the LET will increase rapidly, with LET_d having the steepest curve (Figure 2.3).

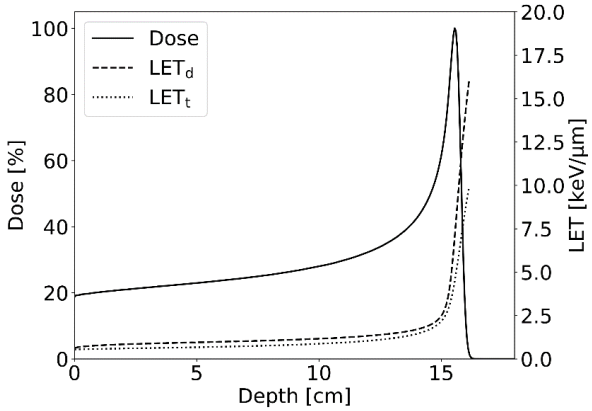

Figure 2.3 Dose (solid line) from a 150 MeV proton beam in water (left y-axis). The corresponding LET_d (dashed line) and LET_t (dotted line) from primary and secondary protons are also shown for dose > 1% (right y-axis). Figure created from Monte Carlo simulations.

2.3 Proton beam parameters

In proton beam therapy, a number of different parameters are used to define a proton beam. The parameters mentioned below are only valid for passively scattered protons where an explicit spread-out Bragg peak (SOBP) is defined. In pencil beam scanning, proton treatment fields are

characterized through each pristine proton pencil beam individually, by specification of the pencil beam energy, weight, direction, spot size etc.

2.3.1 Spread-out Bragg peak

To treat a target volume with protons, a single pristine Bragg peak is usually too narrow to cover the tumor with dose along the beam direction. The solution is to combine several pristine Bragg peaks with decreasing energies and weights to produce an SOBP. The concept of the SOBP was introduced in Robert Wilsons original paper (Wilson, 1946). He suggested that a rotating wheel with steps of variable thickness could be used for the purpose of creating an SOBP. This device is today known as a range modulator (RM) wheel and is widely used in proton therapy (Schippers, 2015).

An SOBP should in general have a flat dose plateau in order to deliver a homogeneous dose to the tumor. This is achieved by properly weighting each individual Bragg peak (Figure 2.4a). The peak with the highest energy is usually the one assigned the highest weight. The range of the most distal peak, *i.e.,* the range of the SOBP, should coincide with the distal end of the target volume. While the range of a proton beam can be defined by the mean projected range (depth of the d80% dose) as touched upon in section 2.1.1, in clinical proton therapy, the range of a proton beam is usually defined at the d90% dose due to historic reasons (Paganetti, 2012). The modulation width of the SOBP determines the length of the dose plateau. The modulation width is specified as the distance from d90% dose to either the proximal 90% (p90%) dose or the p98% dose, depending on the standard chosen by the treatment facility (Figure 2.4a) (Engelsman et al., 2009).

As a result of range straggling and energy spread, the distal part of the SOBP has a certain slope. This is called the distal dose fall-off and is defined as the distance between the positions of the d20% and the d80% dose (Figure 2.4a) (ICRU, 2007).

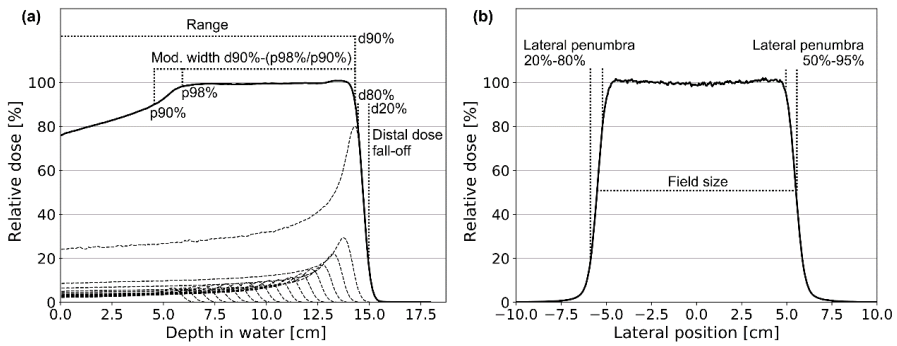

Figure 2.4 (a) Spread-out Bragg peak (SOBP) created from multiple pristine Bragg peaks. Specifications of SOBP range, distal dose fall-off and modulation widths are also illustrated. (b) Lateral profile alongside lateral penumbra definitions. Figures created from Monte Carlo simulations.

2.3.2 Lateral profile and field size

A tumor will also have a certain extension perpendicular to the beam direction. Hence, the beam must also be spread laterally. Techniques for doing that are detailed in section 4.2. It is beneficial to have a sharp lateral penumbra as this makes it possible to spare healthy tissue adjacent the target volume. The lateral penumbra is usually described as the distance between the lateral 20% to 80% dose level, but the distance between the 50%-95% dose levels is also used. Furthermore, the field size is defined as the distance between 50% dose levels (Figure 2.4b) (Lu & Flanz, 2011).

3 Radiobiology

When treating a cancer patient with radiation, the general goal is to kill malignant cancer cells by inactivating their reproductive ability. This is achieved by damaging or destroying the cell DNA. By irradiating cells with ionizing particles, a large number of lesions occur in the DNA. Most of these are in the form of single-strand break (SSB) where either one of the DNA strands are broken or both are broken but with a large separation between the breaks. In SSB, the damage is usually quickly repaired, but incomplete repair may also occur which can lead to cell mutation or cell death. A more ideal form of DNA damage is when the two DNA strands are broken opposite each other or in close proximity. This is termed double-strand break (DSB) and is generally more difficult to repair compared to SSB (Hall & Giaccia, 2012).

In proton therapy, DNA damage can occur when the incident protons or released delta rays hits the DNA. This is called direct action and is more pronounced at higher LET. Another effect is so-called indirect action where protons or delta rays ionize water releasing free radicals which damage the DNA via chemical reactions. This is the most dominant effect at low LET and in conventional photon therapy (Paganetti, 2011b).

The main reason that high LET particles are more biological effective is the spatial distribution of DNA lesions within the cells. Particles with high LET *i.e.*, high ionization density, generates more clustered damage within the DNA compared to low LET particles. Clustered DNA damage is complex and is more difficult to repair compared to the more spatially

distributed ionization tracks within a cell from low LET particles (Paganetti, 2011b).

3.1 The linear quadratic model

The linear quadratic (LQ) model is a very simple mathematical model that has been widely adapted in radiotherapy to describe cell survival (Joiner, 2009). In the model, the fraction of surviving cells S as a function of delivered dose D, can be described by:

$$S(D) = e^{-\alpha D - \beta D^2}, \tag{3.1}$$

where α and β are tissue specific LQ model parameters. A common interpretation of the model is that the linear component $e^{-\alpha D}$ represents damage from so-called single-track events where a single hit is required to inactivate the cell. The quadratic term $e^{-\beta D^2}$ arise from two-track events where two consecutive hits are required to achieve cell-kill (McMahon, 2018). The α/β ratio determines the curvature of the survival curve and reflects the fractionation sensitivity of the cell type or tissue. The unit of the α/β ratio is Gy, and it is equal to the dose level where the linear and quadratic contributions of the survival curve are equal (Figure 3.1).

Tumor tissue and other radiosensitive and early responding tissues such as the skin and bone marrow are generally associated with high α/β ratios. There are, however, many exceptions where for instance prostate tumors (Bentzen & Ritter, 2005) and liposarcomas (Thames & Suit, 1986) have been linked with low α/β ratios. Nevertheless, low ratios are mostly characteristic for late responding tissues such as the central nervous system (Bentzen & Joiner, 2009; McMahon, 2018). While these are general trends

for early and late reacting tissue, it must be emphasized that α/β ratios are often associated with large uncertainties (van Leeuwen et al., 2018).

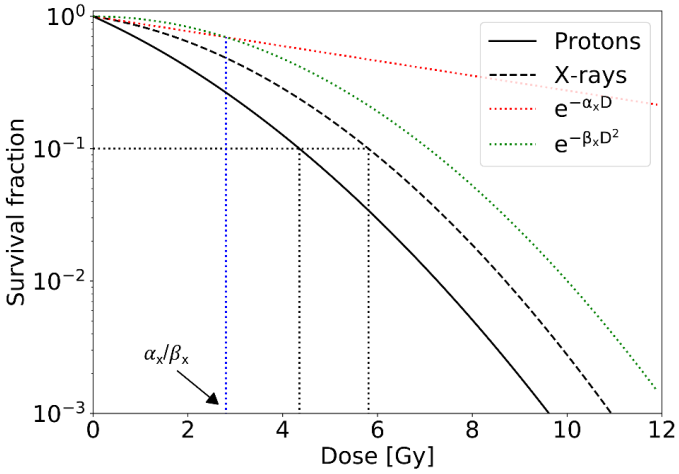

Figure 3.1 Survival fraction curves of V79 cells for x-rays (dashed line) and 11 keV/µm protons (solid line). The red dotted line shows the linear component for the x-rays while the green dotted line shows the quadratic component, resulting in an α/β for x-rays of 2.8 Gy. The black dotted lines represent the RBE at 10% survival, $RBE_{10\%} = \frac{5.8\ Gy}{4.4\ Gy} \approx 1.3$. Figure created using data from Belli et al. (1998).

3.2 Relative biological effectiveness

The relative biological effectiveness (RBE) of protons is defined as the dose from some reference radiation D_x divided by the proton dose D_p to achieve the same biological effect for a specific endpoint. The RBE can be calculated by:

$$RBE = \frac{D_x}{D_p}. \tag{3.2}$$

In proton therapy, the reference radiation is generally photon radiation. Finding isoeffective dose levels for protons and photons for various

endpoints is of great benefit in proton therapy as the vast amount of clinical data for conventional photon therapy can then be exploited and translated to proton treatment. To have a consistent and simple translation, the RBE for protons relative to photons has been set to 1.1 ($RBE_{1.1}$). Hence, protons are considered to be 10% more biologically effective than photons in proton therapy treatments. By multiplying the RBE with the physical proton dose, the so-called biological dose is obtained, also termed the RBE-weighted dose, with unit Gy(RBE) (Paganetti et al., 2019).

The $RBE_{1.1}$ is mainly based on animal experiments conducted in the 1960-70s (G. V. Dalrymple et al., 1966; Glenn V. Dalrymple et al., 1966; Paganetti, 2018; Tepper et al., 1977; Urano et al., 1980). While variations in the RBE were seen, the $RBE_{1.1}$ was deduced as an average value over multiple endpoints, at the center of the target volume and doses of 2 Gy/fraction. It was furthermore decided to use a conservative RBE to ensure tumor control during proton therapy. The $RBE_{1.1}$ has since been adapted by proton therapy clinics around the world.

There has been published a great amount of experimental data of the proton RBE for clonogenic cell survival. Multiple studies analyzing such data have shown a proton RBE dependency on LET, dose level, tissue type, and biological endpoint (Khachonkham et al., 2020; Maeda et al., 2016; Mara et al., 2020; Paganetti, 2014). The analysis by Paganetti (2014) showed that the RBE for a typical SOBP was found to range from 1.1 in the entrance region, to 1.15 in the center, to 1.35 at the distal edge and further up to 1.7 at the distal dose fall-off. A variable RBE could be of

concern if proton treatments based on $RBE_{1.1}$ would lead to either underdosage of the tumor volume or overdosage of healthy tissue.

3.2.1 LET dependency

Radiation effects on a cellular level are highly dependent on the track structure and dosimetric effects on both micro and nano scales. While the LET is a macroscopic quantity that describe the energy loss per unit path length, it is considered a reasonable approximation of the complexity and concentration of the inflicted damage (Paganetti, 2014). As touched upon at the beginning of section 3, for low LET radiation to reach a certain dose level, a large amount of ionization tracks is required, effectively leading to a homogenous distribution of particle tracks and dose deposit. In contrast, due to the increased ionization density from particles of higher LET such as protons, clustered and more severe damage is inflicted on the DNA which is more difficult to repair, effectively leading to an increased RBE (Paganetti, 2011b). The RBE-LET dependency for protons has been demonstrated from cellular experiments (Figure 3.2).

Considering that the LET increases with decreasing proton energy (Figure 2.3), the RBE will also increase, particular in the distal part of the proton beam. This effectively leads to an extension of the biological effective proton beam range of a few millimeters (Paganetti & Goitein, 2000). It is furthermore recognized that the average LET is higher for proton beams of lower ranges as well as smaller modulation widths. The range dependence, although relatively small, can be attributed to the lower energy protons that are required for shorter beam ranges, leading to an increase in the LET. In regards to the modulation width dependency, the LET increases over a

smaller area compared proton beam of longer modulation widths, effectively increasing the RBE at the center of the SOBP (Paganetti, 2014).

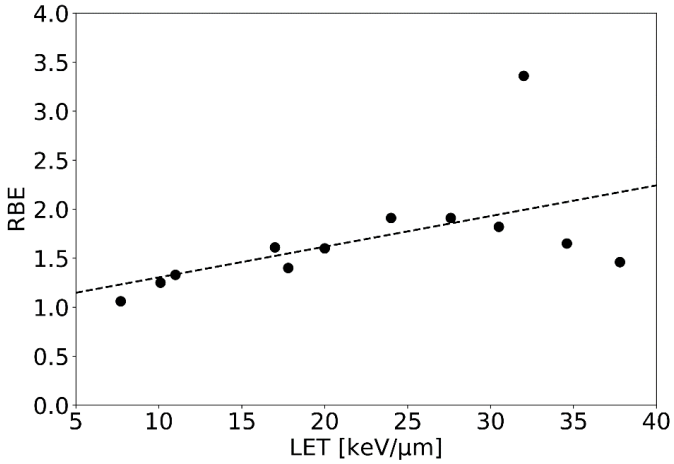

Figure 3.2 Proton RBE at 10% cell survival for V79 cells. The dashed line shows a linear fit. Figure created using data from Sørensen *et al.* (2011).

3.2.2 Tissue dependency

Each cell line or tissue type can be associated with a specific α_x and β_x value from the LQ-model for photon radiation. While there is an expected RBE dependency on tissue type (*i.e.*, on $(\alpha/\beta)_x$), the exact relation is somewhat unclear (Paganetti et al., 2019). There has been published data suggesting that the RBE increases with decreasing $(\alpha/\beta)_x$ only for $(\alpha/\beta)_x < 5$ Gy (Gerweck & Kozin, 1999). The *in vitro* data studied by Paganetti (2014) points to an increase in RBE for decreasing $(\alpha/\beta)_x$ for protons with $\mathrm{LET_d}$ < 15 keV/µm at 2 Gy/fraction. Nevertheless, there are discrepancies in the data, and only a particularly strong dependency is seen for $\mathrm{LET_d} <$ 3 keV/µm and even tendencies of decreasing RBE for decreasing $(\alpha/\beta)_x$ are

seen for higher LET_d values (Paganetti, 2014). It must, however, be emphasized that the data sets studied are largely uncertain.

3.2.3 Dose dependency

By decreasing the dose per fraction there is a tendency of increasing proton RBE for cell survival (Paganetti, 2014). This effect is also illustrated by the more pronounced shoulder in the LQ models survival curve for photons compared to protons (Figure 3.1) and is particularly pronounced at high LET or low $(\alpha/\beta)_x$. Nevertheless, evaluating *in vitro* data in regard to dose dependency is somewhat difficult. Most of the published experimental data have few data points for doses below 2 Gy. Furthermore, assessing cellular survival fractions below 0.1%, which generally occur at high doses, is challenging. The validity of the LQ model below doses of 1 Gy is also questionable (Paganetti et al., 2019).

While the exact relationship of the RBE-dose dependency is not known, the general trend of increasing RBE for lower doses is a concern for critical organs around the distal dose fall-off of the proton beam - an effect that comes in addition to the increased LET in the same region.

3.2.4 Endpoint dependency

The majority of data on the RBE stems from clonogenic cell survival. The RBE is commonly reported using the 10% survival fraction as a biological endpoint (Figure 3.1 and 3.2). However, the RBE will depend on the different survival fractions.

Furthermore, while cell survival may be a good surrogate for predicting the RBE for tumor control, there are other endpoints that may be more relevant, in particular for normal tissue damage (Paganetti et al., 2019).

In vivo data are more closely related to clinical outcome compared to *in vitro* data and could provide better estimates for the RBE in regard to normal tissue damage. However, *in vivo* experiments are more costly and more prone to uncertainties (Paganetti et al., 2019). There do exist *in vivo* experiments (Sørensen et al., 2017; Saager et al., 2018) indicating the same trends for the RBE-LET and RBE-dose dependencies as shown from *in vitro* data, but the RBE is still expected to vary *in vivo* due to differences in biological mechanisms such as immune response and repair mechanisms (Paganetti et al., 2019).

3.2.5 RBE models

Multiple theoretical RBE models have been developed that aim to quantify the RBE variation in proton therapy. These can be divided into three main categories: plan-based models, mechanistic models, and phenomenological models.

Plan-based models are the simplest type. These are not directly based on cell experiments, but rather on data available in the treatment plan such as dose and LET, hence the name plan-based. These models typically assume a certain normalization factor to obtain an RBE of 1.1 in for instance the target volume or in a typical SOBP. While they do not provide RBE values directly based on experimental data, they can give insights into the dosimetric RBE effects of an increased LET, and also illustrate the potential inhomogeneity of the RBE-weighted dose distribution (Paganetti et al., 2019). They are furthermore useful for LET-based treatment plan optimization (Unkelbach et al., 2016).

Mechanistic models seek to explain biological effects by modelling underlying biological processes that lead to lesions or damages on a microscopic scale such as DSBs. These events are further quantified and related to overall cell survival. Different models have been developed such as the local effect model (LEM) (Elsasser et al., 2010; Scholz et al., 1997) and the microdosimetric kinetic model (MKM) (Hawkins, 1998) clinically used in carbon ion therapy in Europe and Japan, respectively.

Phenomenological models are based on empirical data from *in vitro* experiments and make use of the LQ model to quantify cell survival. Not taking microscopic processes into account, the models rely on α and β of the reference radiation as well as the $\mathrm{LET_d}$ and dose levels from experiments. A multitude of models exist in literature (Carabe et al., 2012; McNamara et al., 2015; Rørvik et al., 2017; Wedenberg et al., 2013; Wilkens & Oelfke, 2004a). For an in-depth review of the available models, the reader is referred to Rørvik et al. (2018). The phenomenological models can all be parameterized from the LQ model. Since the proton RBE is defined when the survival fraction for proton radiation S_p equals the survival fraction of the photon radiation S_x, the following relation using equation (3.1) is true:

$$S_p(D_p) = S_x(D_x) \Rightarrow e^{-\alpha D_p - \beta D_p^2} = e^{-\alpha_x D_x - \beta_x D_x^2}, \tag{3.3}$$

where D_p is the physical proton dose, D_x is the photon dose, α_x and β_x are the LQ model parameters for the photons while α and β are parameters for the proton radiation. Combining equations (3.2) and (3.3) the proton RBE can be expressed by:

$$\begin{aligned} &RBE\left(D_p, \alpha, \beta, \left(\frac{\alpha}{\beta}\right)_x\right) \\ &= \frac{1}{2D_p}\left(\sqrt{\left(\frac{\alpha}{\beta}\right)_x^2 + 4D_p\left(\frac{\alpha}{\beta}\right)_x \frac{\alpha}{\alpha_x} + 4D_p^2 \frac{\beta}{\beta_x}} - \left(\frac{\alpha}{\beta}\right)_x\right). \end{aligned} \tag{3.4}$$

In general, the RBE will reach its maximum when the dose approaches zero, and its minimum when the dose goes towards infinity. Thus, the RBE can be derived at the dose extremes:

$$\lim_{D_p \to 0} RBE = RBE_{max} = \frac{\alpha}{\alpha_x}. \tag{3.5}$$

$$\lim_{D_p \to \infty} RBE = RBE_{min} = \sqrt{\frac{\beta}{\beta_x}}. \tag{3.6}$$

These can be inserted into equation (3.4), resulting in:

$$\begin{aligned} &RBE\left(D_p, \left(\frac{\alpha}{\beta}\right)_x, RBE_{max}, RBE_{min}\right) \\ &= \frac{1}{2D_p}\left(\sqrt{\left(\frac{\alpha}{\beta}\right)_x^2 + 4D_p\left(\frac{\alpha}{\beta}\right)_x RBE_{max} + 4D_p^2 RBE_{min}^2} - \left(\frac{\alpha}{\beta}\right)_x\right). \end{aligned} \tag{3.7}$$

Equation (3.7) is common for all the LQ based phenomenological models. They do, however, vary in aspects such as the selection of data points and regression techniques from the cell experiments (Rørvik et al., 2018). A distinction can also be made between models that characterize a linear relationship between the LET_d and RBE, and those that assume a non-linear relationship (Rørvik et al., 2017). In contrast to linear RBE models that can use the LET_d to calculate the RBE, non-linear RBE models require the full LET spectra to quantify the RBE.

3.3 Variable RBE in a clinical setting

While it is well established from both *in vitro* and *in vivo* experiments that the RBE varies depending on the factors outlined in the previous section, it is still a question of how the RBE variability affects clinical treatment of patients, with a particular concern for organs and tissues with low $(\alpha/\beta)_x$ and in areas of increased LET. While treatment facilities are aware of the potential dangers of elevated LET and RBE, a quantitative evaluation is not common, especially considering that not all facilities have access to systems that can calculate LET and RBE. Nevertheless, it is common to try to mitigate the impact of a variable RBE, in particular at the end of the proton range, by taking certain measures. These include careful selection of treatment field angles such that beams do not stop within or near critical organs. Another method is to use an increased number of treatment fields to lower the field weights and thus the RBE uncertainties (Indelicato et al., 2014; Paganetti et al., 2019).

In recent years, a several studies have investigated the correlation between a variable RBE and various clinical endpoints such as radiation necrosis and disease recurrence (Bahn *et al.*, 2020; Bolsi *et al.*, 2020; Eulitz *et al.*, 2019b; Giantsoudi *et al.*, 2016; Niemierko *et al.*, 2021; Peeler *et al.*, 2016; Sethi *et al.*, 2014; Underwood *et al.*, 2018; Wang *et al.*, 2020; Ödén *et al.*, 2020). There is a lot of variation in the studies such as patient cohort sizes, choice of endpoints, diagnoses, and conclusions. Nevertheless, the majority of the studies has been able to find a significant correlation between a variable RBE and the investigated endpoint.

4 Treatment planning and delivery techniques

4.1 Treatment planning

In radiotherapy, regardless of the delivery technique, the goal is to distribute a homogeneous dose to the target volume. At the same time, it is important to minimize the dose to surrounding healthy tissue. This requires careful treatment planning.

One of the first steps in treatment planning is usually to acquire anatomical 3D images of the patient with focus on the treatment area. A prerequisite for radiotherapy treatment is a CT scan to obtain density information of the patient body to allow for calculation of dose distributions. These images are often combined with either MRI images or PET (positron emission tomography) scans to increase soft tissue contrast and to better assess the tumor extent and OARs.

Images from a CT scanner consists of a 3D matrix where each matrix element (*i.e.*, voxel) contains a Hounsfield unit (HU). HUs relate to the attenuation of x-rays during imaging and are affected by the relative electron density in the material. The relationship between the HUs and electron density is not linear and a calibration curve between the two is required for each separate CT scanner (Langen et al., 2015). To create this calibration curve, a common approach is the stochiometric method where measurements of x-ray attenuation in tissue equivalent materials are used (Schneider et al., 1996). In proton therapy, most treatment planning systems are water-based (tissues are modelled as water of different density) and proton beam measurements in treatment facilities are mainly conducted in water.

It is therefore of interest to calibrate the HUs in terms of relative stopping power ratios to water. These ratios can be derived from a combination of the relative electron densities and the Bethe Bloch equation (2.1). The calibration curves are subject to uncertainties, which can be reduced by for instance using dual-energy CT scans or ideally by using proton CT to obtain relative stopping power ratios directly from protons (Langen et al., 2015).

The acquired images from CT, MRI and/or PET form the basis for the delineation of the target volume and organs. ICRU has defined important volumes used in treatment planning such as the gross tumor volume (GTV), clinical target volume (CTV), and planning target volume (PTV). Furthermore, OARs and planning organs at risk volumes (PRV) are usually delineated before patient treatment. The GTV encompass all visible diseased tissue while the CTV comprise of the GTV, but also includes areas with suspected microscopic cancer tissue. The PTV and PRVs adds additional margins to the CTV and OARs, respectively. These margins are defined to account for uncertainties such as patient positioning and internal variation including organ and target movement. In contrast to the GTV and CTV, the margins for the PRVs and PTV are dependent on whether the patient is treated with photons or protons as the latter requires additional margins due to range uncertainties (Li et al., 2015). However, fixed margins have limitations where for instance the PTV margin, while ensuring CTV coverage, might compromise OARs. A technique that is becoming more common is robust optimization where organ motion and uncertainties are incorporated into the treatment plan optimization directly based on the CTV,

making the concept of a PTV obsolete (Chen et al., 2012; Liu et al., 2012; Unkelbach et al., 2018).

Prior to administering dose to the patient, a treatment plan is created using a treatment planning system (TPS). TPSs usually rely on so-called inverse planning where a dose planner assigns dose objectives and dose limits to targets and critical organs, in addition to defining treatment field angles. Based on the applied criteria, the TPS subsequently optimize the treatment plan to provide the best possible dose distribution. A requirement in treatment planning is that the optimization process should be relatively quick. TPSs therefore generally use so-called pencil beam algorithms to calculate the dose distributions (Hong et al., 1996). Such analytical algorithms typically offer an acceptable compromise between calculation time and accuracy.

Most of the relevant information from the treatment plan is stored in a common format called DICOM (Digital Imaging and Communications in Medicine). The DICOM CT Image files store the 3D images acquired from the CT scan. DICOM RT Struct contains information regarding the delineation of targets, OARs, and other regions of interest. The plan created in the TPS is stored in the DICOM RT Plan file containing information such as treatment angles, beam energies, isocenter positions, and depending on the delivery technique, data regarding the aperture and compensator, or spot size data. Lastly, the delivered dose distribution is stored in the DICOM RT Dose file. The dose is scored on a grid defined in the TPS, and dose values in each scoring voxel are located in the RT Dose file (NEMA, 2021). Using a common format such as DICOM, simplifies the translation

of patient and treatment information between different systems and software.

4.2 Delivery techniques

To obtain protons with energies suitable for clinical treatment, powerful accelerators are required. In proton therapy, particle acceleration is generally achieved by either a cyclotron or a synchrotron. There are many differences between the two accelerator types. Cyclotrons usually have a smaller footprint and can provide a continuous beam. However, the maximum beam energy is generally limited at around 250 MeV and to adjust the beam energy of the extracted protons, a physical object in the form of an energy degrader must be placed in the beam path, resulting in a lower energy beam but at the cost of an increased energy spread. Synchrotrons are normally larger compared to cyclotrons. As a result, they can produce proton beams with much higher energies, as well as accelerate heavier particles such as carbon ions to energies suitable for treatment. The beam energy can be adjusted within the accelerator, producing sharp monoenergetic particle beams. On the other hand, synchrotrons are not able to produce continuous beams, but rather beam pulses, ultimately making the energy switching more time consuming (Schippers, 2015).

Proton beam accelerators produce so-called pencil beams with a Gaussian profile of a few millimeters (Slopsema, 2011). Since target volumes generally have a certain extension, the pencil beam must be spread laterally as well as distally after being extracted from the accelerator. This is accomplished in the treatment nozzle, which in many treatment facilities is placed in a rotating gantry in order to irradiate the patient from different angles

(Schippers, 2015). To deliver the proton beam for patient treatment, two beam delivery techniques have been dominating: passive scattering (PS) and pencil beam scanning (PBS).

4.2.1 Passive scattering

Historically, PS has been the most commonly used delivery technique and is still used by many proton therapy facilities (PTCOG, 2021a). By employing different materials and geometrical components in the beam path, the narrow pencil beam is spread laterally as well as shaped according to the target volumes (Figure 4.1a). While different proton therapy vendors have different types of scattering components as well as setups within the nozzle, the lateral spreading of the proton beam is based on the same principle: multiple Coulomb scattering. A passive treatment nozzle usually employs scattering materials of high-Z, such as lead, to achieve a high scattering power relative to the energy loss. PS delivery can be divided into so-called single scattering or double scattering (DS). Single scattering employs less scattering material in the beam path to obtain a relatively narrow and flat proton beam - typically used for treatment of small target volumes such as ocular melanomas. Field sizes in single scattering generally does not exceed a diameter of 7 cm (Slopsema, 2011). In DS, a second additional scatterer is used to further spread the beam to achieve treatment fields with sizes up to about 25 cm in diameter (Lu & Flanz, 2011). A common type of second scatterers are the so-called contoured scatterers. In these, more scattering material is located in the center compared to the outer edge. This results in a larger fraction of the central protons being scattered to the edges, creating a flat profile. However, since the protons reaching the periphery parts of the

scatterer traverse less material, the high-Z contoured scatterer is combined with a low-Z material such as PMMA to have a uniform energy loss across the entire scatterer (Figure 4.1a) (Slopsema, 2011).

A monoenergetic proton beam, *i.e.*, the pristine Bragg peak, is only a few millimeters in depth. As mentioned in section 2.3.1, in order to cover the clinical target volume distally with dose, the depth-dose curve must be widened. This can be done by combining multiple pristine Bragg peaks of decreasing range (energy) and weights, resulting in an SOBP with uniform dose (Figure 2.4a). Depending on the target extent, the size of the uniform dose region can be altered by either adding or reducing the number of pristine Bragg peaks, increasing or decreasing the modulation width, respectively. There are several different techniques to produce an SOBP. The most common method is to use an RM wheel. The wheel has steps of varying thickness corresponding to the range pull-back of each pristine Bragg peak (Figure 4.1a). The angular sizes of the steps vary and determines the weight of each Bragg peak. Generally, the thinnest step has the largest size (and weight) with decreasing size and thickness for each consecutive step. The RM wheel rotates during beam irradiation, resulting in protons traversing the different steps of varying thickness and size leading to an SOBP (Slopsema, 2011). A treatment nozzle usually has several different wheels that can be interchanged in accordance with the requested range and modulation width of the SOBP. However, to create SOBPs with flat dose plateaus for a range of energies using a limited number of RM wheels, a beam current modulation (BCM) is applied to fine tune the weights of the pristine Bragg peaks (Lu & Kooy, 2006). Another method to create SOBPs is to use a ridge

filter. This filter consists of multiple ridges and valleys, where the ridge thicknesses define the pullback of the protons, and the ridge widths determines the weights. Each requested modulation width requires a separate ridge filter, and a library of different filters are usually defined (Mazal et al., 2015).

After the scatterers have spread the beam to a uniform lateral distribution and the RM wheel, or ridge filter, has created an SOBP, the dose must be conformed according to the target area. This is most commonly achieved by using an aperture. The aperture is typically milled from a solid block of brass. The aperture opening is defined according to the target volume with added margins for *e.g.*, setup uncertainties. The aperture material is chosen to provide a high stopping power at a relatively low thickness, designed to stop all particles outside of the opening (Figure 4.1a) (Slopsema, 2011).

A range compensator is used to shape the proton dose to the distal edge of the target volume. It is desirable to have low scattering power and a high stopping power for the compensator. Therefore, it is commonly created from a block of low-Z and (relatively) high density material such as PMMA. The compensator is milled such that protons that are to reach the most distal parts of the target traverse less material compared to protons that stop at shallower depths (Figure 4.1a) (Mazal et al., 2015).

4.2.2 Pencil beam scanning

In PBS, two dipole magnets located in the nozzle are used to steer the beam in order to "paint" the target volume with dose (Figure 4.1b). This is done without the requirement of scattering materials in the beam path as well as collimating components (Flanz, 2011).

During the optimization process in the TPS, the target volume is assigned a certain number of spots covering the entire volume both laterally and distally. Each spot will be allocated a certain weight, size, and position in x, y and z. The x and y (lateral) positions are adjusted by the dipole magnets while the z position is determined by the beam energy. The weights of the spot positions are distributed such that the target receives a homogeneous dose. This is either done on a field-by-field basis called single-field optimization, or the weights are assigned in such a way that the dose becomes homogeneous only when taking all the treatment fields into account, referred to as multi-field optimization or intensity-modulated proton therapy (IMPT).

There are different techniques that can be used to irradiate the spot positions with the pencil beam. Spot scanning is a technique where each spot is irradiated separately, *i.e.*, the beam is turned off between each spot. Another technique is to irradiate each spot in each energy layer continuously such that the beam is only turned off between energy layers. This technique, referred to as raster scanning, is more efficient compared to spot scanning (Zhu et al., 2015). It is, however, important that the optimization algorithm from the TPS considers the transit dose when moving between spots (Inaniwa et al., 2007).

The spots in the target volume are irradiated one energy layer at the time. As there are strict requirements on the spot sizes in PBS, adjusting the beam energy within the nozzle by an RM wheel or ridge filter is not done (Slopsema, 2011). The energy must be adjusted either directly in the case of a synchrotron, or by a degrader at the exit of a cyclotron. The main

disadvantage of these methods is the time it takes to change the energy which is in the order of a couple of seconds (Zhu et al., 2015).

PBS systems are the standard for most new treatment facilities and many current facilities are making a transition from PS to PBS (Mohan *et al.*, 2017a). PBS has many advantages compared to passive scattering such as larger field sizes, less secondary particles such as neutrons, more conformal dose distributions and no patient specific components must be created (Figure 4.1) (Lu & Flanz, 2011; Mohan & Grosshans, 2017; Shin et al., 2009). However, passive scattering is still more robust to patient and organ motion, and it is quicker to deliver the dose after the patient has been positioned on the treatment table.

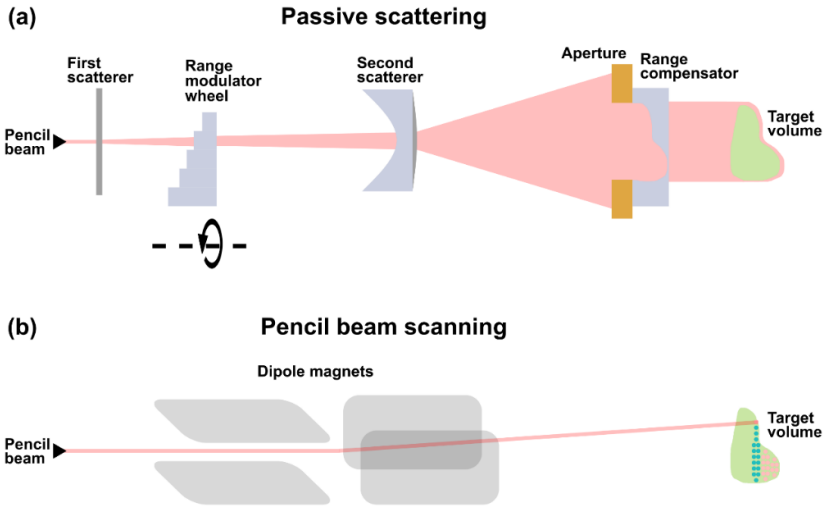

Figure 4.1 In passive scattering (a), a pencil beam is spread laterally and distally using various components. The dose is conformed according to the target volume by apertures and range compensators. In pencil beam scanning (b), the beam steered using dipole magnets. Each spot is irradiated by the pencil beam, and the target volume is distally divided into energy layers. Red spots in the figure represent irradiated spots, while green spots are remaining in the current energy layer.

4.3 Monte Carlo simulations

Analytical pencil beam algorithms used in treatment planning are fast and normally sufficiently accurate for patient dose calculations in proton therapy clinics (Y Jia et al., 2012; Petti, 1996). Nevertheless, they can encounter limitations, especially in low dose regions, in areas of high heterogeneity or in the case of metallic implants (Bueno et al., 2013; Catli & Tanir, 2013; Paganetti et al., 2008; Schuemann et al., 2015; Shin et al., 2017; Yepes et al., 2018). Furthermore, most analytical algorithms that are implemented in proton therapy clinics does not support LET calculation, which is a prerequisite for obtaining variable RBE (Mohan *et al.*, 2017a).

In contrast to analytical dose calculation algorithms, Monte Carlo (MC) simulations use pseudo random sampling from probability density functions (PDFs) to calculate how particles interact through different materials. Instead of estimating dose distributions by modelling pencil beams as an entity, MC codes track each primary particle, including secondary produced particles, separately. The tracking is performed on a step-by-step basis where for each step (typically a small distance) the most probable interaction for the tracked particle is sampled from the PDFs (Paganetti, 2011a).

MC simulations are considered to be the most accurate method of dose calculation. However, the precision, *i.e.*, the statistical uncertainty in MC, is primarily dependent on the number of primary particles simulated. Hence, a large number of particles must be simulated to achieve a given accuracy, which can be very time consuming. This is the main reason why general-purpose MC codes are seldomly used for treatment planning and in daily clinical routine. Nevertheless, general-purpose MC codes are highly versatile

tools for post-treatment simulations and research purposes. They are normally highly customizable and can be used to investigate a number of aspects during treatment such as very low doses, neutron doses, LET and RBE. To build an in-house MC recalculation system, a precise model of the treatment head is generally required. This includes careful calibration of the MC system to either measurements or the TPS (Paganetti, 2011a). Furthermore, facilitating data flow between the TPS and MC considering differences in for instance scoring quantities and coordinate systems is important (Bauer et al., 2014; Verburg et al., 2016).

5 Pediatric brain tumor patients

From 2015 to 2019, an average annual number of 240 patients between the ages of 0 to 19 years old were diagnosed with cancer in Norway. 24% of these diagnoses were cancer in the central nervous system, including brain tumors (Cancer Registry of Norway, 2020). When treating brain tumors with radiotherapy, the brainstem is often at risk of receiving unwanted dose. Thus, keeping the brainstem dose below established dose constraints has a high priority.

5.1 The brainstem in proton therapy

The brainstem is a highly important organ that controls many vital bodily functions. It is located in the posterior fossa (Figure 5.1) and is the connecting structure between the cerebrum and the spinal cord. The brainstem consists of three main substructures: the midbrain, pons, and medulla oblongata. The midbrain controls sensory functions such as visuals and auditory senses, while the pons and medulla oblongata control vital parts including cardiovascular and respiratory systems (OpenStax College, 2013). In addition to the main brainstem substructures, there are also several fiber tracts running from the motor cortex and through the brainstem to the spinal cord. These have all important functional roles such as limb movement and sensory discrimination (Hua et al., 2012).

Due to the brainstem being a very compact organ both structurally and functionally, it is very delicate. Small lesions or other kinds of damage to the brainstem can be devastating and fatal (Standring, 2016).

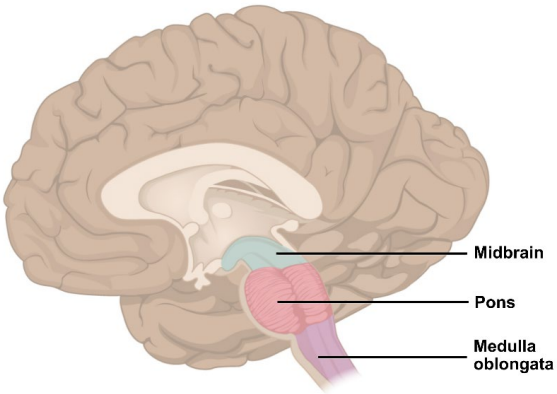

Figure 5.1 Illustration of the brainstem consisting of the midbrain, pons, and medulla oblongata. Figure modified from OpenStax College (2013).

The incidence of symptomatic brainstem toxicity following proton therapy of posterior fossa tumors have been reported between 0% and 16% (Ares et al., 2016; Gentile et al., 2018; Giantsoudi et al., 2016; Gunther et al., 2015; Indelicato et al., 2014; Macdonald et al., 2013; McGovern et al., 2014). Current brainstem tolerance doses are well-established and associated with relative low occurrences of brainstem toxicity of 2.4% among the three largest proton therapy facilities treating pediatric patients in the United States (Haas-Kogan et al., 2018). Nevertheless, since the consequences of brainstem toxicity are so severe, reducing the incidence even further is of great importance.

Proton therapy centers may use slightly different brainstem dose constraints based on institutional clinical experience (Haas-Kogan et al., 2018). There is, however, an ongoing phase III clinical trial (ACNS0831) from the Children's Oncology Group (2010), recommending that the goal for the median dose to the brainstem should be $\leq$ 52.4 Gy(RBE) and must not surpass 54 Gy(RBE), based on data from both photon and proton therapy.

Although certain studies have published specific dose limits to the center of the brainstem (Debus et al., 1997; Indelicato et al., 2014), no official recommendations have been made. Nevertheless, considering that the brainstem is a very heterogeneous organ, it has been suggested that specific regions might be more radiosensitive (Hua et al., 2012; Meeks et al., 2000; Uh et al., 2013).

5.1.1 Specific RBE concerns for the brainstem

As previously mentioned, the LET increases at the distal edge of proton beams, further leading to an increase of the RBE. Brain tumors, and in particular posterior fossa tumors, are often located in vicinity of the brainstem and the variable RBE is therefore of particular concern for such patients. Children with brain tumors are also typically treated with doses below 2 Gy(RBE) per fraction (Bates et al., 2020), a dose level where an increase in the RBE is expected. Furthermore, the brainstem is considered a late-reacting organ and is thus characterized by a low $(\alpha/\beta)_x$. While the specific brainstem $(\alpha/\beta)_x$ value is associated with uncertainties, it is considered to be between 2 and 3 Gy (Clark et al., 1998; Mayo et al., 2010; Meeks et al., 2000; Orton & Cohen, 1988). For such a low $(\alpha/\beta)_x$ the RBE is assumed to increase. Furthermore, in regard to pediatric patients, these children are generally small in size compared to grown adults and are therefore typically treated with low range proton beams with smaller modulation widths. This results in higher LET values, further leading to an increase in the RBE (Marteinsdottir et al., 2019; Paganetti, 2014). All of the listed factors emphasize the concern of the RBE in the brainstem when treating children with brain tumors.

6 Thesis objective

The overall objective of this study was to investigate and explore the effects of LET and variable RBE in the brainstem for pediatric patients treated with proton therapy. Specifically, this also involved a regional analysis of the RBE with regard to the substructures of the brainstem. A prerequisite for obtaining LET and RBE for these patients was to implement a double scattering proton treatment nozzle in a Monte Carlo code. Objectives of each paper included in this thesis are described below.

Paper I

- To investigate how different tumor locations relative to the brainstem influence the LET and variable RBE within the brainstem.
- To investigate how different treatment field setups alters the LET and variable RBE within the brainstem.

Paper II

- To investigate how isodose volumes are influenced by different variable RBE models within both the brainstem and brainstem substructures.

Paper III

- To implement the components of a double scattering treatment nozzle into a Monte Carlo code.
- To develop a system to recalculate and investigate variable RBE-weighted doses within patients treated with double scattering proton therapy.

Paper IV

- To investigate if elevated LET, and thus increased RBE, contributes to symptomatic brainstem toxicity for pediatric brain tumor patients treated with proton therapy.
- To investigate if substructures of the brainstem have different sensitivities to LET and RBE regarding symptomatic brainstem toxicity.

7 Materials and methods

7.1 Patient material and calculation software

All patient data used in this PhD project had been anonymized and originated from the University of Florida Health Proton Therapy Institute (UFHPTI). All treatment plans from UFHPTI were DS proton therapy plans generated in the Eclipse TPS (Varian Medical Systems, Palo Alto, CA, USA). These DS plans were used in Papers III-IV. In Paper I, patient data from UFHPTI were replanned using IMPT in Eclipse at Haukeland University Hospital. In Paper II, the patient data from UFHPTI were replanned using IMPT in Eclipse at Aarhus University Hospital using the same dose constraints and treatment field angles as for the original DS plans.

All IMPT and DS plans in this PhD project were recalculated using the FLUKA Monte Carlo code (Battistoni et al., 2016; Böhlen et al., 2014; Ferrari et al., 2005). So-called FLUKA user routines were used in order to define complex setups regarding properties such as primary particle distributions, scoring quantities, transport events, and dynamic geometry components.

7.2 Recalculation of IMPT plans

To import treatment plan data into the FLUKA Monte Carlo code for recalculation, the CT images as well as plan information must be translated into a format readable for FLUKA. CT data can be directly imported using Flair (Vlachoudis, 2009), a graphical user interface for FLUKA, while the foundation for treatment plan translation and importation had already been

created in Fjæra (2016). Scripts had been developed to generate DAT files containing pencil beam information from DICOM files from the initial treatment plans. The information included spot positions and spot sizes, spot energies and spot weights, as well as pencil beam directions. During recalculation, for each primary particle the FLUKA *source* user routine was called to randomly sample a pencil beam from the treatment plans.

In order to accurately recalculate the treatment plans, the in-house FLUKA recalculation system was calibrated according to the TPS (Paper I). A generic HU to material density calibration curve from the TPS was linked to the CT images before treatment planning. Furthermore, the treatment plans were generated based on a virtual treatment machine called CAP GENERAL, associated with a specific HU to relative stopping power calibration curve. In order to avoid differences in dose distributions due to different calibration curves, both calibration curves were implemented into FLUKA. The HU to material density could be directly imported. For the HU to relative stopping power, a total of 64 artificial phantoms of varying HUs were created and a 160 MeV pristine Bragg peak for each HU was simulated in the TPS. The same simulations were also conducted in FLUKA, the range differences between the TPS and FLUKA were analyzed and stopping power scaling factors reflecting the range differences were employed in FLUKA such that equal ranges for each HU were calculated in both systems. Material definitions for specific HU intervals were defined according to the methods of Schneider et al. (2000) and Parodi et al. (2007).

Energy spreads were approximated to a value of 0.9% of the initial beam energy for the entire energy range in Paper I. In preparation for Paper II,

the energy spreads were tuned and defined as a variable function of the initial beam energy. To define the energy spread calibration curve, eight pristine Bragg peaks with energies between 70-250 MeV were created in the TPS. These were recalculated using an initial energy spread of 0.9% in FLUKA. The width differences between the TPS and FLUKA at the 80% distal dose for each peak were compared. If the width difference was > 1 mm, the energy spread in FLUKA was adjusted and the Bragg peak was re-simulated until differences were below 1 mm.

By default, FLUKA estimates the dose per primary particle. Since clinical dose delivery is based on the total dose, it is desirable to obtain absolute doses in FLUKA. In Papers I and II, the dose from FLUKA was normalized to the mean TPS dose within the PTV.

7.2.1 Scoring dose to water

In order to have an unbiased comparison of the FLUKA dose to the TPS dose, the dose to water (D_w) was obtained in FLUKA. Instead of scoring the FLUKA dose directly *i.e.*, dose to material, the fluence of all particles Φ_i was scored in a grid equal to the one used during the initial treatment planning. Using the *fluscw* user routine, for each particle interaction, the D_w was estimated using the following relation:

$$D_w = \sum_i \frac{LET_{i,w}}{\rho_w} \Phi_i, \tag{7.1}$$

where i specifies the particle type, $LET_{i,w}$ is the unrestricted LET in water for particle i and ρ_w is the water density. The $LET_{i,w}$ is obtained using the

FLUKA *GETLET* function where the density of the material can be overridden to water regardless of the actual material.

7.2.2 Scoring dose-averaged LET

In preparation for Paper I, a method was implemented in FLUKA to obtain the $\mathrm{LET_d}$ using the *fluscw* routine in conjunction with an offline Python script. By utilizing equations (2.8) and (7.1) the $\mathrm{LET_d}$ (in water) in each scoring voxel could be calculated by:

$$LET_d = \frac{\sum_i \frac{LET_{i,w}^2}{\rho_w} \Phi_i}{\sum_i \frac{LET_{i,w}}{\rho_w} \Phi_i}, \tag{7.2}$$

where i only included primary and secondary protons. The quantities in the numerator and denominator were scored separately in FLUKA, while the division was performed offline.

7.2.3 Implementing variable RBE models

Our research group performed a literature search to obtain all phenomenological LQ based RBE models for protons published per November 2017. All models were rephrased to have a common formalism as mentioned in section 3.2.5 and further detailed in Rørvik et al. (2018). This was done in order to simplify both model comparison and the implementation into the FLUKA recalculation system. Since the LQ based linear phenomenological models use the $\mathrm{LET_d}$ to quantify the RBE (Rørvik et al., 2018), the $\mathrm{LET_d}$ from equation (7.2) was used to calculate RBE_{max} and RBE_{min} for the models. These quantities were calculated offline on a voxel-by-voxel basis. Furthermore, the RBE_{max} and RBE_{min}, a user-defined $(\alpha/\beta)_x$ as well as the dose from equation (7.1) (divided by the number of fractions) were

inserted into equation (3.7) to obtain the variable RBE in each voxel for a given model. For the non-linear RBE models that rely on the LET spectrum, RBE_{max} and RBE_{min} were calculated online in the *fluscw* routine using the following equations:

$$RBE_{max} D_w = \sum_i r_{max} \frac{LET_{i,w}}{\rho_w} \Phi_i, \tag{7.3}$$

$$RBE_{min} D_w = \sum_i r_{min} \frac{LET_{i,w}}{\rho_w} \Phi_i, \tag{7.4}$$

where r_{max} and r_{min} are biological weighting functions for a specific non-linear RBE model (Rørvik *et al.*, 2017).

7.2.4 Patient simulations

In Paper I, CT scans of a five-year-old male diagnosed with ependymoma were used as a foundation for the treatment plans. To investigate how tumor location and treatment field angles influence the LET within the brainstem, the target volume was shifted into four different positions relative to the brainstem. A variety of different treatment field angles was also defined as well as different IMPT spot spacings. This resulted in 11 different treatment plans and a total of 33 treatment field each separately simulated using 30 million primary particles.

In Paper II, three pediatric patients with brain tumors were recalculated in FLUKA using 50 million primaries per treatment field. The spatial overlap of isodose curves from variable RBE models using different $(\alpha/\beta)_x$ values were evaluated and compared with isodose curves from $RBE_{1.1}$ doses using so-called Dice similarity coefficients (Dice, 1945).

7.3 Recalculation of DS plans

The majority of methods outlined in the previous section for IMPT including the calculation of D_w, $\mathrm{LET_d}$ and variable RBE were also used when recalculating DS plans.

7.3.1 Implementing and calibrating a treatment nozzle

In order to recalculate the DS plans for patients treated at the UFHPTI, the treatment nozzle had to be implemented into FLUKA (Paper III). The nozzle was a so-called universal nozzle and was installed by IBA (Ion Beam Applications, Belgium). The IBA universal nozzle consists of the following main components that the proton beam interacts with (from upstream to downstream): first ionization chamber, first scatterers, RM wheels, second scatterers, variable collimators, second ionization chamber, field mirror and snouts as well as patient specific apertures and range compensators. Based on blueprints provided by IBA through UFHPTI, the geometry of these components was created in FLUKA (Figure 7.1). While most components could be defined using simple geometry definitions, RM wheels and patient specific components required more advanced solutions.

Each RM wheel in the IBA nozzle is associated with 255 BCM weights that fine-tune the SOBP flatness by specifying the beam intensities. Each BCM weight covers an angle span of $365°/255 \approx 1.43°$. To model a rotating RM wheel, the *source* routine in FLUKA was used to define a weighted random sampling algorithm that emulates a time-dependent rotation. For each primary particle, a BCM weight alongside the specific weight position on the wheel is sampled and the wheel is rotated accordingly. Given

sufficient statistics, this method generates indistinguishable results compared to a continuously time-dependent rotating wheel.

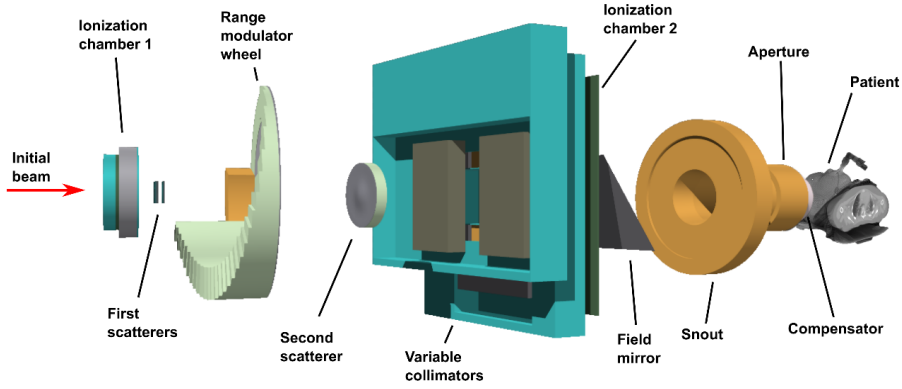

Figure 7.1 The nozzle at UFHPTI implemented in FLUKA. Component distances have been reduced for better visibility. Some components are interchangeable; thus, all component varieties are not shown such as other RM wheels, second scatterers or snouts. Modified from the Flair geometry viewer module.

To generate patient specific apertures and compensators, a Python script was built that automatically creates the components in FLUKA. As FLUKA relies mainly on text-based input, the components were defined using simple ASCII files.

In contrast to the IMPT recalculation system which had been calibrated to the TPS, the DS recalculation system was calibrated towards measurements in water phantoms conducted during the commissioning of the treatment facility back in 2006. Measurement data of ranges from pristine Bragg peaks of various energies were collected. The measurement setups for each Bragg peak were defined in FLUKA and the Bragg peaks were simulated. Range differences between measurements and FLUKA simulations were

registered, and the initial beam energy defined in FLUKA was adjusted accordingly to minimize the range differences. Energy spreads were also calibrated using a similar method as for the IMPT system, however, with a decrease in the permitted differences between FLUKA and measurements. Furthermore, the geometry implementation of the treatment nozzle in FLUKA was verified by comparing SOBPs and lateral profiles from FLUKA and measurements using a variety of ranges and modulation widths, aperture openings, and range compensators.

As the final objective of the DS implementation was to recalculate patients treated at UFHPTI, calibration curves to obtain absolute doses in FLUKA were defined. Furthermore, dose comparisons between FLUKA and the TPS for a set of patients were conducted. While calibration curves for absolute dose can be defined as a simple function of initial beam energy for IMPT (Jakel et al., 2004), in DS the relationship between the dose and the number of primary particles is highly dependent on the range and modulation width for a given SOBP. Thus, multiple calibration curves for small SOBP range spans were defined, where each curve provided the relationship between the modulation width and the number of particles per unit dose.

To reduce the lateral spread in air, patients are typically treated with an air gap as small as feasible, and distances of 2 cm between the patient and the compensator are not unusual. This can lead to an overlap between the compensator and the so-called voxel cage surrounding the patient, which was the case for most patients in Paper IV. This was partly solved by cropping the voxel cage as tightly as possible. However, cropping was sometimes not sufficient, and a two-step simulation method was developed by utilizing

a phase space file. In step one of the phase space simulation, all primary particles are simulated and when a certain particle reaches the downstream part of the compensator, the particle type, position, kinetic energy, as well as direction are recorded into a phase space file using the FLUKA *mgdraw* user routine. In step two, the entire treatment nozzle, including the aperture and compensator, are removed from the simulation environment, and only the patient is included. The *source* routine is used to read each line from the phase space file and particles from the file are subsequently simulated. These particles start within the voxel cage, resolving the issue of overlapping components.

7.3.2 Patient simulations

A total of 36 pediatric brain tumor patients were selected for the case-control study in Paper IV. Each case with symptomatic brainstem injury was matched with three controls based on age (± 1.5 years), diagnosis, adjuvant therapy, and brainstem dose parameters ($D_{10\%}$ ± 2 Gy(RBE), and maximum dose; $D_{0.1cc}$ ± 2 Gy(RBE)). Since many particles stops within the DS nozzle and never reach the patient, each treatment field was simulated using 600 million primary particles to obtain statistical uncertainties below 1% in the target volume. Differences in LET_d, RBE, and variable RBE-weighted doses from RBE models were compared in brainstem and brainstem substructures for cases and controls using metrics as well as volume histograms.

7.4 Ethical considerations

The patient data used in all papers originated from UFHPTI. All patient data were anonymized, and the usage of the patient data was approved by an UFHPTI institutional review board.

8 Summary of results

8.1 Paper I: LET variation depending on tumor location

The evaluated tumor locations relative to the brainstem were full overlap (FO), half overlap (HO), juxtaposed posterior (JP) and 1 cm posterior (1cmP) (Figure 8.1). One posterior and two lateral treatment fields were used.

A high LET_d edge was seen at the distal part of the treatment fields surrounding the tumor volume. For tumor locations JP and 1cmP, the LET_d in the brainstem was most pronounced with mean values of 5.9 keV/μm and 6.6 keV/μm, respectively, compared to a mean LET_d in the brainstem 3.2 keV/μm and 4.5 keV/μm for FO and HO, respectively.

To obtain variations in the biological effect due to LET, the physical dose was multiplied with the LET_d and a factor c (*i.e.*, $RBE_{LET} = 1 + c \cdot LET_d$), termed the LET weighted dose (LWD). The value of c was set to provide a mean RBE of 1.1 within a certain region in the target volume. The highest mean and maximum LWD in the brainstem were seen for the FO case (maximum LWD = 63 Gy(RBE)), with decreasing LWD for increasing distance between tumor and brainstem due to the decrease in physical dose (maximum LWD for 1cmP = 35.5 Gy(RBE) (Figure 8.1).

By changing the treatment field angles for the JP plan, the mean LET_d was reduced to 4.0 keV/μm by using a vertex posterior treatment field in combination with two lateral anterior fields. However, the selected field angles also increased the physical dose slightly compared to the original plan.

The spot spacing was adjusted between 3 to 9 mm. While the mean brainstem LET_d remained unchanged, the 9 mm spot spacing introduced an increase in the LWD of 6%.

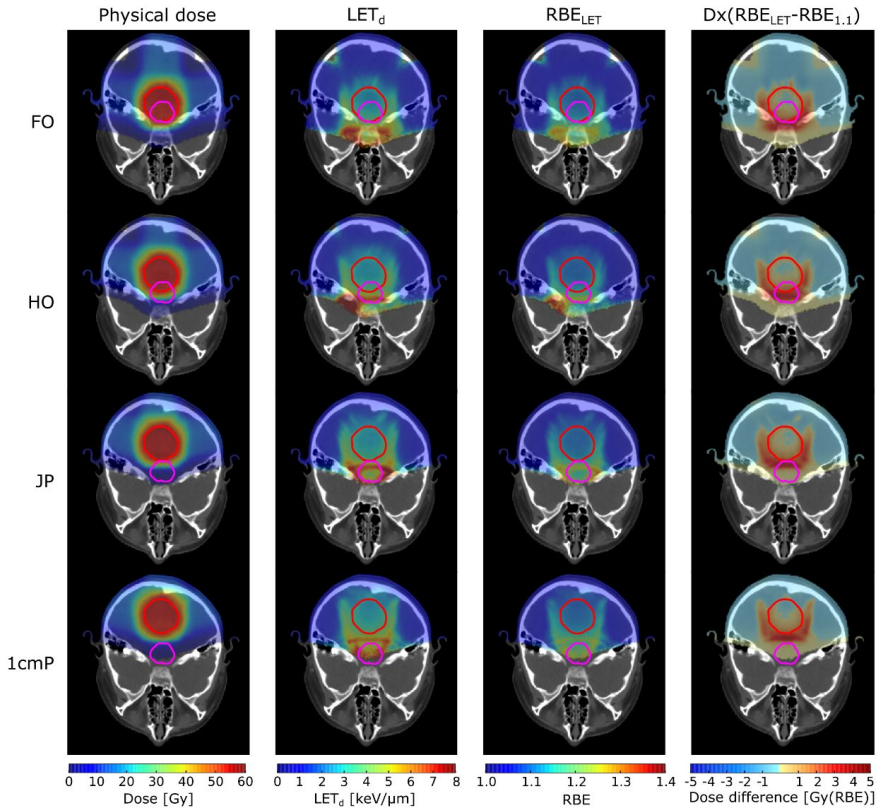

Figure 8.1 Axial view of physical doses, LET_d, RBE_{LET} and dose difference between using $RBE_{1.1}$ and RBE_{LET} for the various tumor locations. Voxels receiving doses below 0.01% of the prescription dose are set transparent. The figure is reprinted from Paper I with permission from Taylor & Francis Group.

8.2 Paper II: Spatial agreement of variable RBE models

The spatial agreement between isodose volumes from $RBE_{1.1}$ and from the phenomenological RBE models of Rørvik et al. (2017) (ROR), McNamara et al. (2015) (MCN), Wedenberg et al. (2013) (WED), Carabe et al. (2012)

(CAR) as well as the plan-based LET-weighted dose (LWD) (Unkelbach et al., 2016) were investigated. The spatial agreement was compared for each 5 Gy(RBE) dose level and quantified using Dice similarity coefficients (DSCs) where DSC = 1 represents full overlap while DSC = 0 represents no overlap. DSCs, doses and RBE were studied for the full brainstem, midbrain, pons, and medulla oblongata in three patients diagnosed with craniopharyngioma, low-grade glioma, and ependymoma.

In general, the spatial agreement between $RBE_{1.1}$ and all the variable RBE models decreased for increasing isodose levels. Furthermore, isodoses from phenomenological models consistently enclosed the $RBE_{1.1}$ isodoses. The LWD also fully enclosed the $RBE_{1.1}$ except for a few isodose levels and structures, where a negligible shift between the isodose curves occurred.

The patient with ependymoma had the largest variation in dosimetric volumes and DSCs across the models. The $V_{50Gy(RBE)}$ in the brainstem increased from 32% using $RBE_{1.1}$ up to 49% for WED. Simultaneously, the spatial agreement showed in this case a DSC of 0.79 for WED, and 0.95 for LWD (Figure 8.2).

The applied $(\alpha/\beta)_x$ values were also varied between 2.1, 2.5 and 3.3 Gy for the phenomenological models, where a considerable decrease in the variable RBE-weighted dose was seen for increasing $(\alpha/\beta)_x$.

Considering that high dose levels introduce decreasing spatial agreement, the effect of a variable RBE is most pronounced for higher dose and small volumes, where constraints commonly are applied in clinical settings.

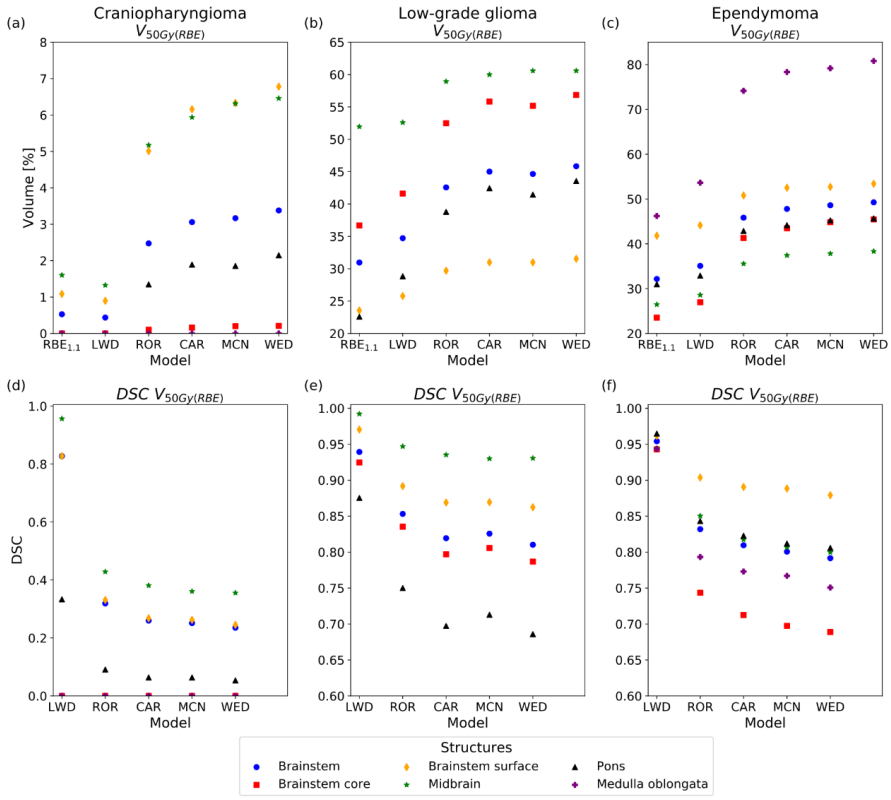

Figure 8.2 $V_{50Gy(RBE)}$ metrics and corresponding Dice similarity coefficients within the full brainstem and brainstem substructures for the three patients. An $(\alpha/\beta)_x$ of 2.1 Gy was used for the phenomenological models. The figure is reprinted from Paper II under the CC BY-NC-ND 4.0 license.

8.3 Paper III: Implementation of a DS nozzle in a MC system

The main components of the DS nozzle at UFHPTI were implemented into the FLUKA Monte Carlo code in Paper III. In order to accurately recalculate treatment plans, the implementation was calibrated and verified by comparisons with measurements conducted in water phantoms.

In general, good agreement between FLUKA and measurements was achieved. Range differences between FLUKA and measurements for pristine Bragg peaks were used for range calibration, and SOBPs were used for range

verification. After calibration, range differences were within ±1 mm for 26 out of 28 investigated SOBPs. Observed differences in modulation widths between FLUKA and measurements were within ±2 mm for 22 of the 28 SOBPs, while the remaining were within ±5 mm (Figure 8.3a).

Verification of the aperture collimation showed an agreement within ±1 mm for 80%-20% lateral penumbras for all aperture openings at several depths (Figure 8.3b). Using a range compensator in FLUKA resulted in range differences within 1 mm when compared to measurements.

Lastly, treatment plans for two previously treated patients were recalculated in FLUKA as a verification procedure, also obtaining LET_d and variable RBE for the patients. The mean PTV dose difference between the TPS and FLUKA for the two patients were between 0.4%-1.4%. Gamma pass rates (3%/3mm) were between 90%-99% in the full brain.

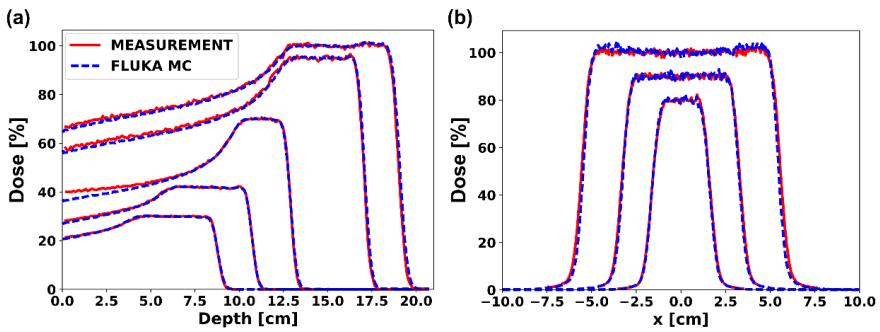

Figure 8.3 (a) Spread-out Bragg peaks for five combinations of ranges and modulation widths. (b) Lateral profiles for 3×3 cm^2, 6×6 cm^2 and 10×10 cm^2 aperture openings. The figure is adapted from Paper III under the CC BY-NC-ND 4.0 license.

8.4 Paper IV: Variable RBE and pediatric brainstem toxicity

The $RBE_{1.1}$ dose, LET_d as well as variable RBE and RBE-weighted doses were investigated in a 1:3 case-control study. The cohort included 36

pediatric brain tumor patients where nine had experienced symptomatic brainstem toxicity. The brainstem substructures: midbrain, pons, and medulla oblongata were delineated. To approximate physiologic fiber tracts, further substructures of the pons were delineated using four transversal zones: pons posterior, pons middle posterior, pons middle anterior, and pons anterior. The variable RBE models included the phenomenological model of Rørvik et al. (2017) (ROR) and the LET-weighted dose (LWD) (Unkelbach et al., 2016).

Median and maximum LET_d were on average greater for cases compared to controls for all substructures as well as the full brainstem (Figure 8.4). Differences between cases and controls generally increased for the maximum LET_d compared to the median. The largest relative of difference of 18% in maximum LET_d between cases and controls occurred for the midbrain and brainstem core.

The median $RBE_{1.1}$ dose for cases was on average slightly higher compared to controls for the majority of substructures. When these substructures were evaluated using the ROR model and LWD the differences between cases and controls increased. For instance, the average difference in dose to the midbrain was 0.7 Gy(RBE) for $RBE_{1.1}$, increasing to 1.5 Gy(RBE) for both ROR and LWD. In contrast, for the remaining structures where the $RBE_{1.1}$ dose was lower for cases compared to controls, these differences decreased when evaluating the RBE-weighted dose using ROR and LWD. These trends were also widely apparent for when comparing cases and controls in each group separately.

Overall, there was a large variation in both LET and RBE within cases and controls, with generally higher LET and RBE in the brainstem for cases. Patients at high risk of brainstem toxicity might therefore benefit from individual assessment of LET/RBE.

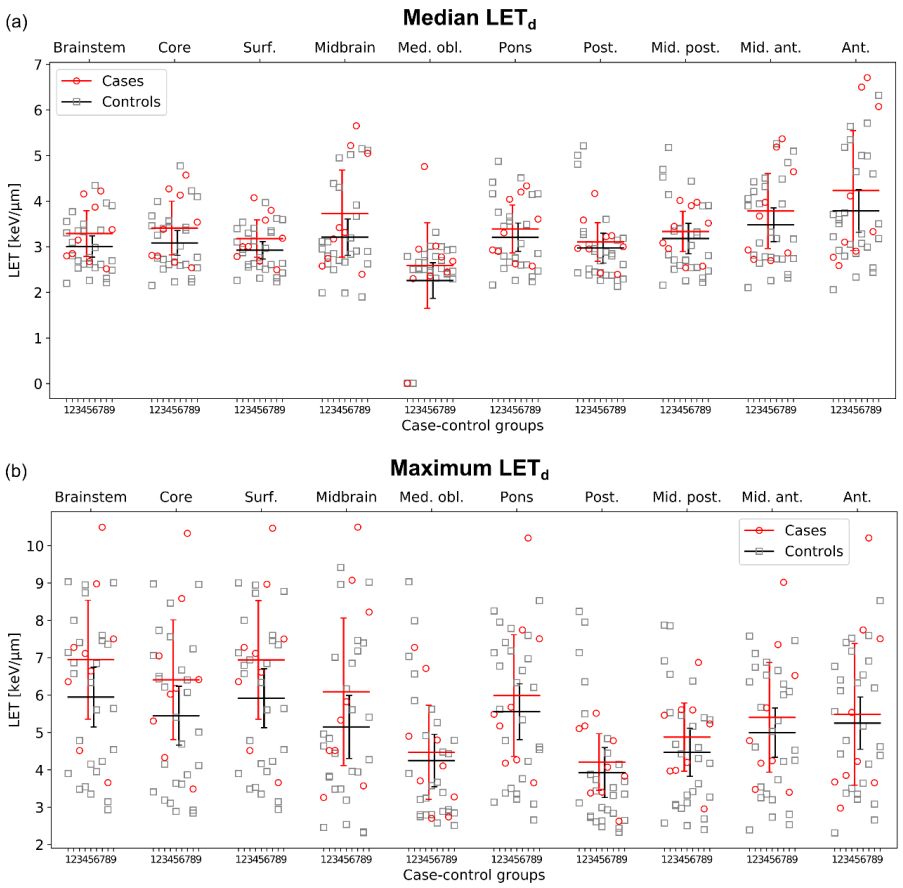

Figure 8.4 Median LET_d (a) and maximum LET_d (b) for cases (red) and controls (gray/black) in relevant structures. Horizontal lines show average values for cases and controls, while the vertical error bars depict 95% confidence intervals. Only the LET_d in voxels receiving doses over 1 Gy($RBE_{1.1}$) has been considered. Abbreviations: Core = Brainstem core, Surf. = Brainstem surface, Med. obl. = Medulla oblongata, Post. = Pons posterior, Mid. post. = Pons middle posterior, Mid. ant. = Pons middle anterior, and Ant. = Pons anterior.

9 Discussion

It is well known, from both *in vitro* and *in vivo* experiments, that the RBE for protons varies with the dose level, tissue type, LET, and biological endpoint. Despite this knowledge, clinical proton therapy practice has been operating with a fixed RBE of 1.1. Considering that the ill-effects of proton therapy have been generally low and clinical evidence of a varying RBE has been absent, the RBE of 1.1 has by many considered an acceptable approximation. However, since 2016, clinical evidence of a variable RBE has begun to emerge - with multiple studies indicating a correlation between radiation toxicity and RBE (Bahn *et al.*, 2020; Bolsi *et al.*, 2020; Eulitz *et al.*, 2019b; Peeler *et al.*, 2016; Underwood *et al.*, 2018; Wang *et al.*, 2020; Ödén *et al.*, 2020).

While clinical practice has been based on a fixed RBE, treatment planners have been aware of the potential dangers of elevated LET and RBE at the end of treatment fields. As a measure to circumvent this threat (as well as proton range uncertainties), beam angles are carefully selected to prevent beams pointing directly towards OARs (Haas-Kogan et al., 2018; Indelicato et al., 2014; Paganetti et al., 2019). However, these measures have been adapted based on passive scattering proton therapy. With the ongoing advancement towards PBS, protons will not only be delivered more precisely, but an increase in both LET values as well as LET hot spots is expected (Grassberger *et al.*, 2011). While adjustment of beam angles is feasible also in PBS (Paper I), without a visual representation of the LET, such measures might prove difficult to conduct without proper visual representation of the

LET. The change towards PBS, coupled with the emerging studies showing the correlation between variable RBE and toxicity, warrants the implementation of LET and variable RBE calculation in proton therapy clinics.

9.1 Does the variable proton RBE have a clinical impact on patients?

As mentioned above, multiple clinical studies have in recent years shown a correlation between toxicity and increased RBE. The majority has studied *asymptomatic* toxicity (Bahn *et al.*, 2020; Bolsi *et al.*, 2020; Eulitz *et al.*, 2019b; Peeler *et al.*, 2016; Underwood *et al.*, 2018; Ödén *et al.*, 2020), characterized as grade 1 based on the Common Terminology Criteria for Adverse Events (CTCAE, 2020), assessed from image changes on either CT or MR images. One study has also identified a correlation between increased RBE and *symptomatic* rib fracture after proton therapy of breast cancer (Wang *et al.*, 2020). Nevertheless, other studies have also investigated the effect of variable RBE on toxicity without finding any clear correlation (Giantsoudi *et al.*, 2016; Niemierko *et al.*, 2021).

There are many factors that complicates the task of acquiring enough patients to detect a significant correlation between RBE and toxicity. In the case of symptomatic toxicity following proton therapy, reported numbers are generally low. Furthermore, for instance in the case of symptomatic brainstem toxicity, symptoms have been reported over two years after the start of treatment (Giantsoudi et al., 2016) which is longer than the follow-up for some patients (Haas-Kogan et al., 2018). Studying asymptomatic toxicity has a contrasting issue as short intervals between surgery and

radiation treatment are associated with a higher risk of image changes (Gunther et al., 2015). Moreover, a challenge for studies of both symptomatic and asymptomatic toxicity is to distinguish between radiation induced injury and tumor progression or recurrence (Luhr *et al.*, 2018a; Mayo *et al.*, 2010). This might have contributed to the relatively low number of patients included in some of the studies. The total number of patients included ranged between 3 (Ödén *et al.*, 2020) to 203 (Wang *et al.*, 2020), and the number of patients with reported toxicity ranged from 3 (Ödén *et al.*, 2020) to 23 (Bahn *et al.*, 2020).

A portion of the studies also designed regression models (Bahn *et al.*, 2020; Eulitz *et al.*, 2019b; Peeler *et al.*, 2016) to predict the probability of image change on a voxel-by-voxel basis. While including many voxels with and without necrosis provides lots of data points, it does not increase the number of patients. Moreover, as pointed out by Niemierko et al. (2021), voxel-based regression models require independence between voxels which is not the case for patients treated with radiotherapy.

In general, a fundamental issue regarding the correlation between LET/RBE and asymptomatic toxicity is that it is difficult to predict if image changes will lead to symptoms (Gunther et al., 2015). This, coupled with the generally low number of patients in the studies, complicates the task of providing indisputable evidence of the clinical impact of the variable RBE. Hence, larger studies and more data on patients, preferably with symptomatic toxicity, are required.

9.2 The need for variable RBE models

Phenomenological RBE models are based on *in vitro* experiments using clonogenic cell survival as an endpoint (Rørvik et al., 2018). It is, however, well-known that the RBE varies across different endpoints, and with that comes many associated uncertainties. An ongoing discussion is how relatable the RBE for cell survival is to damage to normal tissue (Haas-Kogan *et al.*, 2018). It is uncertain to what degree the RBE for cell survival can be associated with late effects such as lung fibrosis or spinal cord injury. Nevertheless, studies have indicated a correlation between RBE and lung fibrosis for proton therapy patients (Underwood *et al.*, 2018) and *in vivo* experiments on rat spinal cords have shown higher RBE for increasing LET (Saager *et al.*, 2018). Furthermore, considering that the experiments for cell survival typically have been conducted at doses above 2 Gy, it is expected that RBE for normal tissues and OARs could be higher since these are typically located in regions of low dose, as well as high LET. Normal tissues are also often associated with low $(\alpha/\beta)_x$ values further increasing the RBE (Paganetti et al., 2019).

The RBE calculated from phenomenological RBE models is influenced by the selected α_x and β_x or simply the $(\alpha/\beta)_x$ ratio. These parameters are associated with large uncertainties (van Leeuwen et al., 2018). For instance, the brainstem $(\alpha/\beta)_x$ ratio has been estimated to be 2.1, 2.5 and 3.3 Gy (Mayo *et al.*, 2010). While these values are not that far apart, the difference in the median RBE in the brainstem between using $(\alpha/\beta)_x = 2.1$ and 3.3 could be as much as 20% for variable RBE models, as demonstrated in Paper II. Furthermore, as different tissues and tumors are associated with

different $(\alpha/\beta)_x$ ratios, it might become challenging to select which $(\alpha/\beta)_x$ ratio to use for RBE modelling when such tissues are overlapping.

Bearing in mind the abovementioned uncertainties of variable RBE models, the current practice of RBE of 1.1 does not avoid the issues regarding $(\alpha/\beta)_x$ uncertainties, dose, endpoint or LET dependencies, it merely disregards them. While both the RBE of 1.1 as well as phenomenological models are based on biological data (the former deducted as an average value), the variable RBE models at least quantifies an increase in RBE for elevated LET - a relationship that is difficult to dispute. Although the data sets used by RBE models have large uncertainties, focus on reducing these uncertainties for future experiments should be emphasized to improve the RBE models.

For instance, many studies on *in vitro* experiments have not reported LET values, and some have also neglected to report α and β values. This has resulted in the necessity of simulating the LET as well as fitting the curves to obtain the α and β values (Paganetti, 2014). Consistent experimental setup and proper reporting of dose, LET and α and β are therefore measures that can be taken to reduce uncertainties in the data sets (Paganetti et al., 2019).

Furthermore, in order to create RBE models better suited for normal tissue damage prediction, more relevant data sets in the form of *in vivo* experiments could be used. Indeed, recent *in vivo* experiments have also indicated a correlation between LET and RBE (Sørensen et al., 2017; Saager et al., 2018). However, it should be mentioned that *in vivo* experiments are not only much more costly, but also more difficult to conduct consistently

(Paganetti et al., 2019; Sørensen, 2019). Sufficiently accurate *in vivo* RBE values might therefore prove challenging to obtain (Haas-Kogan et al., 2018).

As shown in Paper II, also supported by other studies (Bertolet & Carabe-Fernandez, 2020; Giovannini et al., 2016; Pedersen et al., 2017; Yepes et al., 2019; Ödén et al., 2017), published RBE models estimate considerable different RBE values, and does not necessarily follow the same dependencies, in particular for $(\alpha/\beta)_x$ (McMahon, 2021; Rørvik *et al.*, 2018). If current *in vitro* based RBE models were to be implemented in a clinical setting, differences among the RBE models could be an obstacle. However, the selection of data points by many of the models are often limited, and both data points and model assumptions can be irrelevant for a clinical setting. By applying specific criteria for data points and dependencies that best reflect a clinical scenario, the number of appropriate RBE models can be substantially reduced (Otterlei *et al.*, 2021). Furthermore, many of the clinically relevant models strongly correlate on the LET dependency, however, with significant disagreement regarding $(\alpha/\beta)_x$ values (McMahon, 2021).

A common argument against using phenomenological RBE models in clinical research is the lack of clinical validation. This is unfortunate, as by not including current RBE models for clinical data studies, validation will never be attained (McMahon, 2021). For instance, many studies investigating the correlation between RBE and toxicity have excluded the usage of phenomenological RBE models and rather used LET or LET-weighted dose, exclusively. While this approach avoids the potential uncertainties that are associated with many RBE models, and in particular $(\alpha/\beta)_x$ uncertainties, opportunities in coupling current models with toxicity in a clinical aspect are

also missed. By including multiple RBE models on large patient groups in toxicity studies, certain models may stand out as better predictors for various endpoints.

9.3 Implementing LET and RBE calculation in clinics

To obtain LET and variable RBE for clinical treatment scenarios, software capable of obtaining such quantities must be available at proton facilities. In this PhD project, the FLUKA Monte Carlo code (Battistoni et al., 2016; Böhlen et al., 2014; Ferrari et al., 2005) was used to estimate dose, LET and RBE. Other alternative MC codes include MCNPX (Los Alamos National Laboratory, 2002), Geant4 (Agostinelli et al., 2003) and TOPAS (Perl et al., 2012). A prerequisite of using MC codes for these purposes is that treatment facility specific information such as beam line geometry and beam information must be implemented and commissioned, in particular for passive scattering proton therapy as was done in Paper III. This is generally regarded as a time consuming and resource intensive process. Nevertheless, as the benefits are significant, it has still been done at several proton treatment facilities (Engelsman et al., 2009; Grevillot et al., 2011; Herault et al., 2005; Lutz et al., 2021; Newhauser et al., 2005; Paganetti et al., 2004; Parodi et al., 2012; Prusator et al., 2017; Sayah et al., 2013; Shin et al., 2017). In addition, the implemented IMPT recalculation system (Paper I) has also been used in multiple studies from our research group (Dahle et al., 2020; Otterlei et al., 2021; Rørvik et al., 2018; Ytre-Hauge et al., 2020), investigating aspects not feasible in standard treatment planning systems.

Perhaps the biggest disadvantage of using Monte Carlo simulations in a clinical setting is the required calculation time necessary for a sufficiently low statistical uncertainty. In particular for passive scattering proton therapy, the majority of the primary particles are stopped in the treatment nozzle. It is, however, possible to reduce calculation times by employing different variance reduction techniques such as particle splitting and Russian roulette (Eulitz *et al.*, 2019a; Mendez *et al.*, 2015; Ramos-Mendez *et al.*, 2013). Furthermore, GPU-based MC algorithms are also beginning to gain popularity, offering a tremendous decrease in calculation time, comparable to analytical algorithms (Beltran et al., 2016; Giantsoudi et al., 2015; X Jia et al., 2012).

There have also been published both analytical (Bertolet et al., 2020; Choi et al., 2018; Sanchez-Parcerisa et al., 2016; Wilkens & Oelfke, 2003) as well as simplified MC based algorithms (Yepes et al., 2019) for calculating LET and RBE. Furthermore, while standard available treatment planning systems does not support calculating LET or variable RBE (Luhr *et al.*, 2018b; Mohan & Grosshans, 2017), there is ongoing development regarding implementing such capabilities in TPSs (Bertolet et al., 2020; Ödén et al., 2017). Nevertheless, it is important to keep in mind that by not using full Monte Carlo, calculation time will be reduced at the cost of precision.

9.4 Scoring of quantities

In proton therapy, the LET_d is the most commonly applied method of averaging the LET and most phenomenological RBE models depends on the LET_d (Rørvik et al., 2018). The LET_d is often considered the most appropriate averaging method for RBE modelling since dose is also closely related

to the biological effect of particles (Grun et al., 2019). For these reasons, the LET_d as well as LET spectra (for non-linear RBE models) were used exclusively in this PhD project. The alternative, LET_t, is considered to be more relevant at higher LET radiation such as carbon ions which have a reduced number of particle tracks compared to protons (Grassberger & Paganetti, 2011).

Furthermore, the LET was scored only considering primary and secondary protons. A recent review by Kalholm et al. (2021) found that the majority of published studies involving quantification of the RBE for protons used LET counting only primary and secondary protons. There is, however, no obvious consensus on which particles to include. Grassberger and Paganetti (2011) have demonstrated the importance of including secondary protons for LET calculations. Another study has showed that by neglecting to consider heavier ions, the LET could be up to 50% lower compared to when including all particles (Grzanka et al., 2018). While there is not necessarily a specific LET that is more correct than others, the most important factor is to be consistent and to accurately report the averaging method and included particles for the LET calculation (Kalholm *et al.*, 2021).

Dose to water has traditionally been reported in radiotherapy (Liu et al., 2002). Scoring quantities in water in Monte Carlo codes has certain advantages. As clinical experience and dosimetric protocols in radiotherapy are water based, scoring the same quantity in MC codes makes it easier to relate the results to clinical experience. Although dose to water in proton therapy has been reported up to 10% higher compared to dose to medium in areas of high density, differences were generally within 1% for normal

density tissue (Paganetti, 2009). For comparison purposes, the dose to water was scored throughout this PhD project. Naturally, the LET to water instead of LET to medium was therefore also scored, although significant differences between water-based and medium-based LET for bony material have been reported as well (Wilkens & Oelfke, 2004b). Hence, by neglecting the elemental composition of the medium, the improved accuracy of MC codes might be slightly reduced.

For all patient recalculations, quantities were scored volumetrically using the same grid and resolution as used during the initial treatment planning. Scoring grid voxels from TPSs are typically larger compared to CT voxels. Larger voxels have the advantage of increasing tracking efficiency for Monte Carlo. Furthermore, by using the same grid for the MC calculations and the TPS, voxel-by-voxel comparisons are simpler to achieve. However, it is important to keep in mind that by scoring on a grid that is not equal to the CT grid, scoring voxels may contain CT voxels of different material compositions. This requires that the MC code defines an average material composition within the scoring voxel, a process that is not always well defined (Paganetti et al., 2008).

9.5 Should current clinical practice be revised?

Using a constant RBE simplifies dose calculation and keeps consistency between treatment facilities. Moreover, if the RBE of 1.1 was to be discarded, it is not clear what new fixed RBE or which variable RBE model to use. As previously mentioned, variable RBE models still lacks clinical validation. Using the incorrect RBE model may not only lead to overdosage of healthy tissue, but also underdosage of the tumor.

While there are indications of a variable RBE both *in vitro*, *in vivo* and from clinical investigation, over 150 000 patients have been treated based on an RBE of 1.1 with no unreasonable numbers of reported toxicities (Luhr *et al.*, 2018b). Nevertheless, the relatively low incidence of toxicity from historical data may be partly attributed to the clinical practice of avoiding beams stopping directly in front of critical organs. Furthermore, when higher than expected toxicity has emerged, a practice has been to reduce prescription doses (Mohan *et al.*, 2017b). While such measures might lead to decreased normal tissue damage, it may also compromise tumor control, limiting the true potential of proton therapy, and potentially masking the consequences of an increased RBE.

Furthermore, the proton therapy community is currently undergoing a progression from passive scattering proton therapy to PBS, and more specifically IMPT. As mentioned, while IMPT increases the dose conformity it also leads to higher LET values (Grassberger *et al.*, 2011). This might compromise the dosimetric advantage of IMPT when considering the variable RBE-weighted dose (Giantsoudi *et al.*, 2018). Moreover, while the effects of LET and variable RBE from current published studies are not entirely concise, new advancements in proton therapy such as image guidance will further increase the dose precision and reduce the potentially smeared-out LET values. Such advancements might increase the effects of the variable RBE (Luhr *et al.*, 2018a).

IMPT also provides the ability to increase the difference in biological effect for normal tissue and tumors by so-called LET optimization. By optimizing each individual beam spot, high LET can be moved and maximized

inside the target region and/or minimized inside critical organs, while still maintaining the physical dose distribution within the target (Cao *et al.*, 2017; Giantsoudi *et al.*, 2013; Grassberger & Paganetti, 2017; Inaniwa *et al.*, 2017; Unkelbach *et al.*, 2016). The MD Anderson Cancer Center has initiated an ongoing phase 1 clinical trial investigating the use of LET optimization for pediatric patients with ependymoma (MD Anderson Cancer Center, 2018).

While proton therapy clinics might not yet be ready to disregard the RBE of 1.1, clinics should start the implementation of LET and variable RBE calculation for plan evaluation and as a visualization tool. With the increasing number of patients treated with proton therapy, more data on LET and RBE can then be collected over time that can be used to revise and improve current RBE models, and in particular provide valuable data for studies on the clinical impact of a variable RBE. Furthermore, patients at high risk of fatal toxicity would clearly benefit from individual assessment of LET and variable RBE, which is demonstrated in Paper IV.

10 Conclusions

Consideration of the LET and variable RBE is particularly important for children with brain tumors. These tumors are often located in close proximity of the brainstem, a critical organ for vital life functions. Great variation in the LET in the brainstem was seen dependent on the relative location of the tumor and brainstem. While altering field angles reduced the LET, it could also slightly increase the physical dose, indicating that accounting for LET and variable RBE-weighted dose clinically may prove difficult without tools allowing for quantitative and visual representation.

Comparing multiple RBE models with $RBE_{1.1}$ for pediatric brain tumor patients revealed that isodose volumes using variable RBE models generally surrounded $RBE_{1.1}$ isodose volumes. The degree of spatial agreement was dependent on the RBE model, the applied model specific parameters, and with a substantial decrease in agreement for increasing isodose levels. Considering that current $RBE_{1.1}$ dose constraints are often defined for high doses and small volumes, developing RBE model specific dose constraints are therefore crucial for dose optimization based on variable RBE models.

To enable extraction of LET and variable RBE data from previously treated patients, a double scattering nozzle was implemented and commissioned in a Monte Carlo code. The implementation was validated to measurement data and provides a powerful tool for studies on long-term follow-up data, including LET and variable RBE.

The nozzle implementation was used in a retrospective case-control study of LET and variable RBE and brainstem toxicity. There were large

interpatient variations in LET/RBE, but general trends pointed to higher LET and RBE for cases compared to controls. The results warrant individual LET/RBE assessment for high-risk patients.

The results from this thesis demonstrate the need for clinical implementation of LET and variable RBE calculation to use for plan evaluation. Clinical access to LET/RBE calculation tools would simplify and increase the quality of assessing and reducing LET and RBE in critical organs, which patients at high risk of toxicity could benefit from. More clinical data on LET and RBE will also be of great value to improve future proton therapy treatment.

Bibliography

Agostinelli, S, Allison, J, Amako, K, Apostolakis, J, Araujo, H, Arce, P, Asai, M, Axen, D, Banerjee, S, Barrand, G, et al. (2003). GEANT4-a simulation toolkit. *Nuclear Instruments & Methods in Physics Research Section a-Accelerators Spectrometers Detectors and Associated Equipment*, *506*(3), 250-303. https://doi.org/10.1016/S0168-9002(03)01368-8

Ares, C, Albertini, F, Frei-Welte, M, Bolsi, A, Grotzer, M A, Goitein, G, & Weber, D C. (2016). Pencil beam scanning proton therapy for pediatric intracranial ependymoma. *J Neurooncol*, *128*(1), 137-145. https://doi.org/10.1007/s11060-016-2090-4

Bahn, E, Bauer, J, Harrabi, S, Herfarth, K, Debus, J, & Alber, M. (2020). Late Contrast Enhancing Brain Lesions in Proton-Treated Patients With Low-Grade Glioma: Clinical Evidence for Increased Periventricular Sensitivity and Variable RBE. *Int J Radiat Oncol Biol Phys*, *107*(3), 571-578. https://doi.org/10.1016/j.ijrobp.2020.03.013

Barton, M B, Jacob, S, Shafiq, J, Wong, K, Thompson, S R, Hanna, T P, & Delaney, G P. (2014). Estimating the demand for radiotherapy from the evidence: a review of changes from 2003 to 2012. *Radiother Oncol*, *112*(1), 140-144. https://doi.org/10.1016/j.radonc.2014.03.024

Bates, J E, Indelicato, D J, Morris, C G, Rotondo, R L, & Bradley, J A. (2020). Visual decline in pediatric survivors of brain tumors following radiotherapy. *Acta Oncol*, *59*(10), 1257-1262. https://doi.org/10.1080/0284186X.2020.1803500

Battistoni, G, Bauer, J, Boehlen, T T, Cerutti, F, Chin, M P, Dos Santos Augusto, R, Ferrari, A, Ortega, P G, Kozlowska, W, Magro, G, et al. (2016). The FLUKA Code: An Accurate Simulation Tool for Particle Therapy. *Front Oncol*, *6*(May), 116. https://doi.org/10.3389/fonc.2016.00116

Bauer, J, Sommerer, F, Mairani, A, Unholtz, D, Farook, R, Handrack, J, Frey, K, Marcelos, T, Tessonnier, T, Ecker, S, et al. (2014). Integration and evaluation of automated Monte Carlo simulations in the clinical practice of scanned proton and carbon ion beam

therapy. *Phys Med Biol*, *59*(16), 4635-4659. https://doi.org/10.1088/0031-9155/59/16/4635

Belli, M, Cera, F, Cherubini, R, Dalla Vecchia, M, Haque, A M, Ianzini, F, Moschini, G, Sapora, O, Simone, G, Tabocchini, M A, et al. (1998). RBE-LET relationships for cell inactivation and mutation induced by low energy protons in V79 cells: further results at the LNL facility. *Int J Radiat Biol*, *74*(4), 501-509. https://doi.org/10.1080/095530098141375

Beltran, C, Tseung, H W C, Augustine, K E, Bues, M, Mundy, D W, Walsh, T J, Herman, M G, & Laack, N N. (2016). Clinical Implementation of a Proton Dose Verification System Utilizing a GPU Accelerated Monte Carlo Engine. *Int J Part Ther*, *3*(2), 312-319. https://doi.org/10.14338/IJPT-16-00011.1

Bentzen, S M, & Joiner, M C. (2009). The linear-quadratic approach in clincal practice. In M C Joiner & A J Van Der Kogel (Eds.), *Basic Clinical Radiobiology* (4th ed., pp. 120-134). Hodder Arnold.

Bentzen, S M, & Ritter, M A. (2005). The alpha/beta ratio for prostate cancer: what is it, really? *Radiother Oncol*, *76*(1), 1-3. https://doi.org/10.1016/j.radonc.2005.06.009

Berger, M J, Coursey, J S, Zucker, M A, & Chang, J. (2017). *Stopping-Power & Range Tables for Electrons, Protons, and Helium Ions*. National Institute of Standards and Technology. https://doi.org/10.18434/T4NC7P

Bertolet, A, & Carabe-Fernandez, A. (2020). Clinical implications of variable relative biological effectiveness in proton therapy for prostate cancer. *Acta Oncol*, *59*(10), 1171-1177. https://doi.org/10.1080/0284186X.2020.1762928

Bertolet, A, Cortes-Giraldo, M A, Souris, K, & Carabe, A. (2020). A kernel-based algorithm for the spectral fluence of clinical proton beams to calculate dose-averaged LET and other dosimetric quantities of interest. *Med Phys*, *47*(6), 2495-2505. https://doi.org/10.1002/mp.14108

Bethe, H. (1930). Zur Theorie des Durchgangs schneller Korpuskularstrahlen durch Materie. *Ann Phys*, *397*(3), 325-400. https://doi.org/10.1002/andp.19303970303

Bhatia, S, & Sklar, C. (2002). Second cancers in survivors of childhood cancer. *Nat Rev Cancer*, *2*(2), 124-132. https://doi.org/10.1038/nrc722

Bloch, F. (1933a). Bremsvermögen von Atomen mit mehreren Elektronen. *Z Phys*, *81*(5-6), 363-376. https://doi.org/10.1007/bf01344553

Bloch, F. (1933b). Zur Bremsung rasch bewegter Teilchen beim Durchgang durch Materie. *Ann Phys*, *408*(3), 285-320. https://doi.org/10.1002/andp.19334080303

Bolsi, A, Placidi, L, Pica, A, Ahlhelm, F J, Walser, M, Lomax, A J, & Weber, D C. (2020). Pencil beam scanning proton therapy for the treatment of craniopharyngioma complicated with radiation-induced cerebral vasculopathies: A dosimetric and linear energy transfer (LET) evaluation. *Radiother Oncol*, *149*, 197-204. https://doi.org/10.1016/j.radonc.2020.04.052

Bueno, M, Paganetti, H, Duch, M A, & Schuemann, J. (2013). An algorithm to assess the need for clinical Monte Carlo dose calculation for small proton therapy fields based on quantification of tissue heterogeneity. *Med Phys*, *40*(8), 081704. https://doi.org/10.1118/1.4812682

Böhlen, T T, Cerutti, F, Chin, M P W, Fassò, A, Ferrari, A, Ortega, P G, Mairani, A, Sala, P R, Smirnov, G, & Vlachoudis, V. (2014). The FLUKA Code: Developments and Challenges for High Energy and Medical Applications. *Nucl Data Sheets*, *120*, 211-214. https://doi.org/10.1016/j.nds.2014.07.049

Cancer Registry of Norway. (2020). *Cancer in Norway 2019 - Cancer incidence, mortality, survival and prevalence in Norway*. Oslo: Cancer Registry of Norway.

Cao, W, Khabazian, A, Yepes, P P, Lim, G, Poenisch, F, Grosshans, D R, & Mohan, R. (2017). Linear energy transfer incorporated intensity modulated proton therapy optimization. *Phys Med Biol*, *63*(1), 015013. https://doi.org/10.1088/1361-6560/aa9a2e

Carabe, A, Moteabbed, M, Depauw, N, Schuemann, J, & Paganetti, H. (2012). Range uncertainty in proton therapy due to variable biological effectiveness. *Phys Med Biol*, *57*(5), 1159-1172. https://doi.org/10.1088/0031-9155/57/5/1159

Catli, S, & Tanir, G. (2013). Experimental and Monte Carlo evaluation of Eclipse treatment planning system for effects on dose distribution of the hip prostheses. *Med Dosim*, *38*(3), 332-336. https://doi.org/10.1016/j.meddos.2013.03.005

Chen, W, Unkelbach, J, Trofimov, A, Madden, T, Kooy, H, Bortfeld, T, & Craft, D. (2012). Including robustness in multi-criteria optimization

for intensity-modulated proton therapy. *Phys Med Biol*, *57*(3), 591-608. https://doi.org/10.1088/0031-9155/57/3/591

Children's Oncology Group. (2010). *Maintenance Chemotherapy or Observation Following Induction Chemotherapy and Radiation Therapy in Treating Patients With Newly Diagnosed Ependymoma*. clinicaltrials.gov. Identifier: ACNS0831. https://clinicaltrials.gov/ct2/show/NCT01096368

Choi, K, Mein, S B, Kopp, B, Magro, G, Molinelli, S, Ciocca, M, & Mairani, A. (2018). FRoG-A New Calculation Engine for Clinical Investigations with Proton and Carbon Ion Beams at CNAO. *Cancers (Basel)*, *10*(11). https://doi.org/10.3390/cancers10110395

Clark, B G, Souhami, L, Pla, C, Al-Amro, A S, Bahary, J P, Villemure, J G, Caron, J L, Olivier, A, & Podgorsak, E B. (1998). The integral biologically effective dose to predict brain stem toxicity of hypofractionated stereotactic radiotherapy. *Int J Radiat Oncol Biol Phys*, *40*(3), 667-675. https://doi.org/10.1016/s0360-3016(97)00734-7

CTCAE. (2020). *Common Terminology Criteria for Adverse Events (CTCAE)*. National Cancer Institute. https://ctep.cancer.gov/protocolDevelopment/electronic_applications/ctc.htm

Dahle, T J, Rusten, E, Stokkevåg, C H, Silvoniemi, A, Mairani, A, Fjæra, L F, Rørvik, E, Henjum, H, Wright, P, Boer, C G, et al. (2020). The FLUKA Monte Carlo code coupled with an OER model for biologically weighted dose calculations in proton therapy of hypoxic tumors. *Phys Med*, *76*, 166-172. https://doi.org/10.1016/j.ejmp.2020.07.003

Dalrymple, G V, Lindsay, I R, Ghidoni, J J, Hall, J D, Mitchell, J C, Kundel, H L, & Morgan, I L. (1966). Some Effects of 138-Mev Protons on Primates. *Radiat Res*, *28*(2), 471-488. https://doi.org/10.2307/3572210

Dalrymple, G V, Lindsay, I R, Hall, J D, Mitchell, J C, Ghidoni, J J, Kundel, H L, & Morgan, I L. (1966). The Relative Biological Effectiveness of 138-Mev Protons as Compared to Cobalt-60 Gamma Radiation. *Radiat Res*, *28*(2), 489-506. https://doi.org/10.2307/3572211

Debus, J, Hug, E B, Liebsch, N J, O'Farrel, D, Finkelstein, D, Efird, J, & Munzenrider, J E. (1997). Brainstem tolerance to conformal

radiotherapy of skull base tumors. *Int J Radiat Oncol Biol Phys*, *39*(5), 967-975. https://doi.org/10.1016/s0360-3016(97)00364-7

Dice, L R. (1945). Measures of the Amount of Ecologic Association between Species. *Ecology*, *26*(3), 297-302. https://doi.org/10.2307/1932409

Elsasser, T, Weyrather, W K, Friedrich, T, Durante, M, Iancu, G, Kramer, M, Kragl, G, Brons, S, Winter, M, Weber, K J, et al. (2010). Quantification of the relative biological effectiveness for ion beam radiotherapy: direct experimental comparison of proton and carbon ion beams and a novel approach for treatment planning. *Int J Radiat Oncol Biol Phys*, *78*(4), 1177-1183. https://doi.org/10.1016/j.ijrobp.2010.05.014

Engelsman, M, Lu, H M, Herrup, D, Bussiere, M, & Kooy, H M. (2009). Commissioning a passive-scattering proton therapy nozzle for accurate SOBP delivery. *Med Phys*, *36*(6), 2172-2180. https://doi.org/10.1118/1.3121489

Eulitz, J, Lutz, B, Wohlfahrt, P, Dutz, A, Enghardt, W, Karpowitz, C, Krause, M, Troost, E G C, & Luhr, A. (2019a). A Monte Carlo based radiation response modelling framework to assess variability of clinical RBE in proton therapy. *Phys Med Biol*, *64*(22), 225020. https://doi.org/10.1088/1361-6560/ab3841

Eulitz, J, Troost, E G C, Raschke, F, Schulz, E, Lutz, B, Dutz, A, Lock, S, Wohlfahrt, P, Enghardt, W, Karpowitz, C, et al. (2019b). Predicting late magnetic resonance image changes in glioma patients after proton therapy. *Acta Oncol*, *58*(10), 1536-1539. https://doi.org/10.1080/0284186X.2019.1631477

Ferrari, A, Sala, P R, Fassó, A, & Ranft, J. (2005). FLUKA : A Multi-Particle Transport Code. CERN-2005-10, INFN/TC_05/11, SLAC-R-773, https://www.slac.stanford.edu/pubs/slacreports/reports16/slac-r-773.pdf

Fjæra, L F. (2016). *Development of a Monte Carlo based treatment planning verification tool for particle therapy* [Master's thesis, University of Bergen]. Bergen. https://bora.uib.no/bora-xmlui/handle/1956/12582

Flanz, J. (2011). Particle Beam Scanning. In H Paganetti (Ed.), *Proton Therapy Physics* (1st ed., pp. 157-190). CRC Press. https://doi.org/10.1201/b11448

Gentile, M S, Yeap, B Y, Paganetti, H, Goebel, C P, Gaudet, D E, Gallotto, S L, Weyman, E A, Morgan, M L, MacDonald, S M, Giantsoudi, D, et al. (2018). Brainstem Injury in Pediatric Patients With Posterior Fossa Tumors Treated With Proton Beam Therapy and Associated Dosimetric Factors. *Int J Radiat Oncol Biol Phys*, *100*(3), 719-729. https://doi.org/10.1016/j.ijrobp.2017.11.026

Gerweck, L E, & Kozin, S V. (1999). Relative biological effectiveness of proton beams in clinical therapy. *Radiother Oncol*, *50*(2), 135-142. https://doi.org/10.1016/s0167-8140(98)00092-9

Giantsoudi, D, Adams, J, MacDonald, S, & Paganetti, H. (2018). Can differences in linear energy transfer and thus relative biological effectiveness compromise the dosimetric advantage of intensity-modulated proton therapy as compared to passively scattered proton therapy? *Acta Oncol*, *57*(9), 1259-1264. https://doi.org/10.1080/0284186X.2018.1468090

Giantsoudi, D, Grassberger, C, Craft, D, Niemierko, A, Trofimov, A, & Paganetti, H. (2013). Linear energy transfer-guided optimization in intensity modulated proton therapy: feasibility study and clinical potential. *Int J Radiat Oncol Biol Phys*, *87*(1), 216-222. https://doi.org/10.1016/j.ijrobp.2013.05.013

Giantsoudi, D, Schuemann, J, Jia, X, Dowdell, S, Jiang, S, & Paganetti, H. (2015). Validation of a GPU-based Monte Carlo code (gPMC) for proton radiation therapy: clinical cases study. *Phys Med Biol*, *60*(6), 2257-2269. https://doi.org/10.1088/0031-9155/60/6/2257

Giantsoudi, D, Sethi, R V, Yeap, B Y, Eaton, B R, Ebb, D H, Caruso, P A, Rapalino, O, Chen, Y E, Adams, J A, Yock, T I, et al. (2016). Incidence of CNS Injury for a Cohort of 111 Patients Treated With Proton Therapy for Medulloblastoma: LET and RBE Associations for Areas of Injury. *Int J Radiat Oncol Biol Phys*, *95*(1), 287-296. https://doi.org/10.1016/j.ijrobp.2015.09.015

Giovannini, G, Bohlen, T, Cabal, G, Bauer, J, Tessonnier, T, Frey, K, Debus, J, Mairani, A, & Parodi, K. (2016). Variable RBE in proton therapy: comparison of different model predictions and their influence on clinical-like scenarios. *Radiat Oncol*, *11*(1), 68. https://doi.org/10.1186/s13014-016-0642-6

Gottschalk, B. (2004). *Passive Beam Spreading in Proton Radiation Therapy*. https://gray.mgh.harvard.edu/attachments/article/212/pbs.pdf

Gottschalk, B. (2011). Physics of Proton Interactions in Matter. In H Paganetti (Ed.), *Proton Therapy Physics* (1st ed., pp. 19-60). CRC Press. https://doi.org/10.1201/b11448

Grassberger, C, & Paganetti, H. (2011). Elevated LET components in clinical proton beams. *Phys Med Biol*, *56*(20), 6677-6691. https://doi.org/10.1088/0031-9155/56/20/011

Grassberger, C, & Paganetti, H. (2017). Varying relative biological effectiveness in proton therapy: knowledge gaps versus clinical significance. *Acta Oncol*, *56*(6), 761-762. https://doi.org/10.1080/0284186X.2017.1316516

Grassberger, C, Trofimov, A, Lomax, A, & Paganetti, H. (2011). Variations in linear energy transfer within clinical proton therapy fields and the potential for biological treatment planning. *Int J Radiat Oncol Biol Phys*, *80*(5), 1559-1566. https://doi.org/10.1016/j.ijrobp.2010.10.027

Grevillot, L, Bertrand, D, Dessy, F, Freud, N, & Sarrut, D. (2011). A Monte Carlo pencil beam scanning model for proton treatment plan simulation using GATE/GEANT4. *Phys Med Biol*, *56*(16), 5203-5219. https://doi.org/10.1088/0031-9155/56/16/008

Grun, R, Friedrich, T, Traneus, E, & Scholz, M. (2019). Is the dose-averaged LET a reliable predictor for the relative biological effectiveness? *Med Phys*, *46*(2), 1064-1074. https://doi.org/10.1002/mp.13347

Grzanka, L, Ardenfors, O, & Bassler, N. (2018). Monte Carlo Simulations of Spatial Let Distributions in Clinical Proton Beams. *Radiat Prot Dosimetry*, *180*(1-4), 296-299. https://doi.org/10.1093/rpd/ncx272

Guan, F, Peeler, C, Bronk, L, Geng, C, Taleei, R, Randeniya, S, Ge, S, Mirkovic, D, Grosshans, D, Mohan, R, et al. (2015). Analysis of the track- and dose-averaged LET and LET spectra in proton therapy using the geant4 Monte Carlo code. *Med Phys*, *42*(11), 6234-6247. https://doi.org/10.1118/1.4932217

Gunther, J R, Sato, M, Chintagumpala, M, Ketonen, L, Jones, J Y, Allen, P K, Paulino, A C, Okcu, M F, Su, J M, Weinberg, J, et al. (2015). Imaging Changes in Pediatric Intracranial Ependymoma Patients Treated With Proton Beam Radiation Therapy Compared to Intensity Modulated Radiation Therapy. *Int J Radiat Oncol Biol Phys*, *93*(1), 54-63. https://doi.org/10.1016/j.ijrobp.2015.05.018

Hall, E J, & Giaccia, A J. (2012). *Radiobiology for the radiologist* (7th ed.). Wolters Kluwer Health/Lippincott Williams & Wilkins.

Hawkins, R B. (1998). A microdosimetric-kinetic theory of the dependence of the RBE for cell death on LET. *Med Phys*, *25*(7 Pt 1), 1157-1170. https://doi.org/10.1118/1.598307

Herault, J, Iborra, N, Serrano, B, & Chauvel, P. (2005). Monte Carlo simulation of a protontherapy platform devoted to ocular melanoma. *Med Phys*, *32*(4), 910-919. https://doi.org/10.1118/1.1871392

Highland, V L. (1975). Some Practical Remarks on Multiple-Scattering. *Nucl Instrum Methods*, *129*(2), 497-499. https://doi.org/10.1016/0029-554x(75)90743-0

Hong, L, Goitein, M, Bucciolini, M, Comiskey, R, Gottschalk, B, Rosenthal, S, Serago, C, & Urie, M. (1996). A pencil beam algorithm for proton dose calculations. *Phys Med Biol*, *41*(8), 1305-1330. https://doi.org/10.1088/0031-9155/41/8/005

Hua, C, Merchant, T E, Gajjar, A, Broniscer, A, Zhang, Y, Li, Y, Glenn, G R, Kun, L E, & Ogg, R J. (2012). Brain tumor therapy-induced changes in normal-appearing brainstem measured with longitudinal diffusion tensor imaging. *Int J Radiat Oncol Biol Phys*, *82*(5), 2047-2054. https://doi.org/10.1016/j.ijrobp.2011.03.057

Haas-Kogan, D, Indelicato, D, Paganetti, H, Esiashvili, N, Mahajan, A, Yock, T, Flampouri, S, MacDonald, S, Fouladi, M, Stephen, K, et al. (2018). National Cancer Institute Workshop on Proton Therapy for Children: Considerations Regarding Brainstem Injury. *Int J Radiat Oncol Biol Phys*, *101*(1), 152-168. https://doi.org/10.1016/j.ijrobp.2018.01.013

ICRU. (2007). ICRU Report 78 - Prescribing, Recording, and Reporting Proton-Beam Therapy. *J ICRU*, *7*(2), 1-222. https://doi.org/10.1093/jicru/ndi004

ICRU. (2011). ICRU Report 85 - Fundamental Quantities and Units for Ionizing Radiation (Revised). *J ICRU*, *11*(1), 1-35. https://doi.org/10.1093/jicru/ndr012

Inaniwa, T, Furukawa, T, Tomitani, T, Sato, S, Noda, K, & Kanai, T. (2007). Optimization for fast-scanning irradiation in particle therapy. *Med Phys*, *34*(8), 3302-3311. https://doi.org/10.1118/1.2754058

Inaniwa, T, Kanematsu, N, Noda, K, & Kamada, T. (2017). Treatment planning of intensity modulated composite particle therapy with dose and linear energy transfer optimization. *Phys Med Biol*, *62*(12), 5180-5197. https://doi.org/10.1088/1361-6560/aa68d7

Indelicato, D J, Flampouri, S, Rotondo, R L, Bradley, J A, Morris, C G, Aldana, P R, Sandler, E, & Mendenhall, N P. (2014). Incidence and dosimetric parameters of pediatric brainstem toxicity following proton therapy. *Acta Oncol*, *53*(10), 1298-1304. https://doi.org/10.3109/0284186X.2014.957414

Jakel, O, Hartmann, G H, Karger, C P, Heeg, P, & Vatnitsky, S. (2004). A calibration procedure for beam monitors in a scanned beam of heavy charged particles. *Med Phys*, *31*(5), 1009-1013. https://doi.org/10.1118/1.1689011

Jia, X, Schumann, J, Paganetti, H, & Jiang, S B. (2012). GPU-based fast Monte Carlo dose calculation for proton therapy. *Phys Med Biol*, *57*(23), 7783-7797. https://doi.org/10.1088/0031-9155/57/23/7783

Jia, Y, Beltran, C, Indelicato, D J, Flampouri, S, Li, Z, & Merchant, T E. (2012). Proton therapy dose distribution comparison between Monte Carlo and a treatment planning system for pediatric patients with ependymoma. *Med Phys*, *39*(8), 4742-4747. https://doi.org/10.1118/1.4736413

Joiner, M C. (2009). Quantifying cell kill and survival. In M Joiner & A Van Der Kogel (Eds.), *Basic Clinical Radiobiology* (4th ed., pp. 41-55). Hodder Arnold.

Kalholm, F, Grzanka, L, Traneus, E, & Bassler, N. (2021). A Systematic Review on the Usage of Averaged LET in Radiation Biology for Particle Therapy. *Radiother Oncol*. https://doi.org/10.1016/j.radonc.2021.04.007

Kassam, A, Widger, K, & Benini, F. (2018). Epidemiology of Suffering in Childhood Cancer. In *Palliative Care in Pediatric Oncology* (pp. 1-12). Springer International Publishing. https://doi.org/10.1007/978-3-319-61391-8_1

Khachonkham, S, Mara, E, Gruber, S, Preuer, R, Kuess, P, Dorr, W, Georg, D, & Clausen, M. (2020). RBE variation in prostate carcinoma cells in active scanning proton beams: In-vitro measurements in comparison with phenomenological models. *Phys Med*, *77*(August), 187-193. https://doi.org/10.1016/j.ejmp.2020.08.012

Langen, K, Polf, J, & Schulte, R. (2015). Imaging for Proton Therapy. In I J Das & H Paganetti (Eds.), *Principles and Practice of Proton Beam Therapy* (1st ed., pp. 165-189). Medical Physics Publishing, Inc.

Li, H, Giebeler, A, Dong, L, Zhang, X, Poenisch, F, Sahoo, N, Gillin, M T, & Zhu, X R. (2015). Treatment planning for Passive Scattering Proton Therapy. In I J Das & H Paganetti (Eds.), *Principles and Practice of Proton Beam Therapy* (1st ed., pp. 647-666). Medical Physics Publishing, Inc.

Liu, H H, Keall, P, & Hendee, W R. (2002). Dm rather than Dw should be used in Monte Carlo treatment planning. *Med Phys*, *29*(5), 922-924. https://doi.org/10.1118/1.1473137

Liu, W, Zhang, X, Li, Y, & Mohan, R. (2012). Robust optimization of intensity modulated proton therapy. *Med Phys*, *39*(2), 1079-1091. https://doi.org/10.1118/1.3679340

Los Alamos National Laboratory. (2002). *MCNPX user's Manual Version 2.3.0*. Report LA-UR-02-2607. https://mcnp.lanl.gov/pdf_files/la-ur-02-2607.pdf

Lu, H-M, & Flanz, J. (2011). Characteristics of Clinical Proton Beams. In H Paganetti (Ed.), *Proton Therapy Physics* (1st ed., pp. 103-123). CRC Press. https://doi.org/10.1201/b11448

Lu, H M, & Kooy, H. (2006). Optimization of current modulation function for proton spread-out Bragg peak fields. *Med Phys*, *33*(5), 1281-1287. https://doi.org/10.1118/1.2188072

Luhr, A, von Neubeck, C, Krause, M, & Troost, E G C. (2018a). Relative biological effectiveness in proton beam therapy - Current knowledge and future challenges. *Clin Transl Radiat Oncol*, *9*(February), 35-41. https://doi.org/10.1016/j.ctro.2018.01.006

Luhr, A, von Neubeck, C, Pawelke, J, Seidlitz, A, Peitzsch, C, Bentzen, S M, Bortfeld, T, Debus, J, Deutsch, E, Langendijk, J A, et al. (2018b). "Radiobiology of Proton Therapy": Results of an international expert workshop. *Radiother Oncol*, *128*(1), 56-67. https://doi.org/10.1016/j.radonc.2018.05.018

Lutz, B, Eulitz, J, Haneke-Swanson, R, Enghardt, W, & Luhr, A. (2021). Precision modeling of the IBA Universal Nozzle double scattering mode at the University Proton Therapy Dresden for Monte Carlo simulation. *J Instrum*, *16*(3), T03007. https://doi.org/10.1088/1748-0221/16/03/T03007

Macdonald, S M, Sethi, R, Lavally, B, Yeap, B Y, Marcus, K J, Caruso, P, Pulsifer, M, Huang, M, Ebb, D, Tarbell, N J, et al. (2013). Proton radiotherapy for pediatric central nervous system ependymoma: clinical outcomes for 70 patients. *Neuro Oncol*, *15*(11), 1552-1559. https://doi.org/10.1093/neuonc/not121

Maeda, K, Yasui, H, Matsuura, T, Yamamori, T, Suzuki, M, Nagane, M, Nam, J M, Inanami, O, & Shirato, H. (2016). Evaluation of the relative biological effectiveness of spot-scanning proton irradiation in vitro. *J Radiat Res*, *57*(3), 307-311. https://doi.org/10.1093/jrr/rrv101

Mara, E, Clausen, M, Khachonkham, S, Deycmar, S, Pessy, C, Dorr, W, Kuess, P, Georg, D, & Gruber, S. (2020). Investigating the impact of alpha/beta and LETd on relative biological effectiveness in scanned proton beams: An in vitro study based on human cell lines. *Med Phys*, *47*(8), 3691-3702. https://doi.org/10.1002/mp.14212

Marteinsdottir, M, Schuemann, J, & Paganetti, H. (2019). Impact of uncertainties in range and RBE on small field proton therapy. *Phys Med Biol*, *64*(20), 205005. https://doi.org/10.1088/1361-6560/ab448f

Mayo, C, Yorke, E, & Merchant, T E. (2010). Radiation associated brainstem injury. *Int J Radiat Oncol Biol Phys*, *76*(3 Suppl), S36-41. https://doi.org/10.1016/j.ijrobp.2009.08.078

Mazal, A, Patriarca, A, Wessels, C, & Das, I J. (2015). Field Shaping: Scattered Beam. In I J Das & H Paganetti (Eds.), *Principles and Practice of Proton Beam Therapy* (1st ed., pp. 191-208). Medical Physics Publishing, Inc.

McGovern, S L, Okcu, M F, Munsell, M F, Kumbalasseriyil, N, Grosshans, D R, McAleer, M F, Chintagumpala, M, Khatua, S, & Mahajan, A. (2014). Outcomes and acute toxicities of proton therapy for pediatric atypical teratoid/rhabdoid tumor of the central nervous system. *Int J Radiat Oncol Biol Phys*, *90*(5), 1143-1152. https://doi.org/10.1016/j.ijrobp.2014.08.354

McMahon, S J. (2018). The linear quadratic model: usage, interpretation and challenges. *Phys Med Biol*, *64*(1), 01TR01. https://doi.org/10.1088/1361-6560/aaf26a

McMahon, S J. (2021). Proton RBE models: commonalities and differences. *Phys Med Biol*, *66*(4), 04NT02. https://doi.org/10.1088/1361-6560/abda98

McNamara, A L, Schuemann, J, & Paganetti, H. (2015). A phenomenological relative biological effectiveness (RBE) model for proton therapy based on all published in vitro cell survival data. *Phys Med Biol*, *60*(21), 8399-8416. https://doi.org/10.1088/0031-9155/60/21/8399

MD Anderson Cancer Center. (2018). *LET Optimized IMPT in Treating Pediatric Patients With Ependymoma*. clinicaltrials.gov. Identifier: NCT03750513. https://clinicaltrials.gov/ct2/show/NCT03750513

Meeks, S L, Buatti, J M, Foote, K D, Friedman, W A, & Bova, F J. (2000). Calculation of cranial nerve complication probability for acoustic neuroma radiosurgery. *Int J Radiat Oncol Biol Phys*, *47*(3), 597-602. https://doi.org/10.1016/s0360-3016(00)00493-4

Mendez, J R, Perl, J, Schumann, J, Shin, J, Paganetti, H, & Faddegon, B. (2015). Improved efficiency in Monte Carlo simulation for passive-scattering proton therapy. *Phys Med Biol*, *60*(13), 5019-5035. https://doi.org/10.1088/0031-9155/60/13/5019

Mohan, R, Das, I J, & Ling, C C. (2017a). Empowering Intensity Modulated Proton Therapy Through Physics and Technology: An Overview. *Int J Radiat Oncol Biol Phys*, *99*(2), 304-316. https://doi.org/10.1016/j.ijrobp.2017.05.005

Mohan, R, & Grosshans, D. (2017). Proton therapy - Present and future. *Adv Drug Deliv Rev*, *109*, 26-44. https://doi.org/10.1016/j.addr.2016.11.006

Mohan, R, Peeler, C R, Guan, F, Bronk, L, Cao, W, & Grosshans, D R. (2017b). Radiobiological issues in proton therapy. *Acta Oncol*, *56*(11), 1367-1373. https://doi.org/10.1080/0284186X.2017.1348621

Molière, G. (1947). Theorie der Streuung schneller geladener Teilchen I Einzelstreuung am abgeschirmten Coulomb-Feld. *Z Naturforsch*, *2A*, 133-145. https://doi.org/10.1515/zna-1947-0302

Molière, G. (1948). Theorie der Streuung schneller geladenen Teilchen II Mehrfach- und Vielfachstreuung. *Z Naturforsch*, *3A*, 78-97. https://doi.org/10.1515/zna-1948-0203

Moyers, M F, Coutrakon, G B, Ghebremedhin, A, Shahnazi, K, Koss, P, & Sanders, E. (2007). Calibration of a proton beam energy monitor. *Med Phys*, *34*(6), 1952-1966. https://doi.org/10.1118/1.2717382

NEMA. (2021). *Digital Imaging and Communications in Medicine (DICOM) Standard*. https://www.dicomstandard.org/

Newhauser, W, Koch, N, Hummel, S, Ziegler, M, & Titt, U. (2005). Monte Carlo simulations of a nozzle for the treatment of ocular tumours with high-energy proton beams. *Phys Med Biol*, *50*(22), 5229-5249. https://doi.org/10.1088/0031-9155/50/22/002

Niemierko, A, Schuemann, J, Niyazi, M, Giantsoudi, D, Maquilan, G, Shih, H A, & Paganetti, H. (2021). Brain Necrosis in Adult Patients After Proton Therapy: Is There Evidence for Dependency on Linear Energy Transfer? *Int J Radiat Oncol Biol Phys*, *109*(1), 109-119. https://doi.org/10.1016/j.ijrobp.2020.08.058

Oeffinger, K C, Mertens, A C, Sklar, C A, Kawashima, T, Hudson, M M, Meadows, A T, Friedman, D L, Marina, N, Hobbie, W, Kadan-Lottick, N S, et al. (2006). Chronic health conditions in adult survivors of childhood cancer. *N Engl J Med*, *355*(15), 1572-1582. https://doi.org/10.1056/NEJMsa060185

OpenStax College. (2013). *Anatomy and Physiology*. Rice University. https://openstax.org/details/books/anatomy-and-physiology

Orton, C G, & Cohen, L. (1988). A unified approach to dose-effect relationships in radiotherapy. I: Modified TDF and linear quadratic equations. *Int J Radiat Oncol Biol Phys*, *14*(3), 549-556. https://doi.org/10.1016/0360-3016(88)90273-8

Otterlei, O M, Indelicato, D J, Toussaint, L, Ytre-Hauge, K S, Pilskog, S, Fjæra, L F, Rørvik, E, Pettersen, H E S, Muren, L P, Lassen-Ramshad, Y, et al. (2021). Variation in relative biological effectiveness for cognitive structures in proton therapy of pediatric brain tumors. *Acta Oncol*, *60*(2), 267-274. https://doi.org/10.1080/0284186X.2020.1840626

Paganetti, H. (2009). Dose to water versus dose to medium in proton beam therapy. *Phys Med Biol*, *54*(14), 4399-4421. https://doi.org/10.1088/0031-9155/54/14/004

Paganetti, H. (2011a). Monte Carlo Simulations. In H Paganetti (Ed.), *Proton Therapy Physics* (1st ed., pp. 265-304). CRC Press. https://doi.org/10.1201/b11448

Paganetti, H. (2011b). The Physics of Proton Biology. In H Paganetti (Ed.), *Proton Therapy Physics* (1st ed., pp. 593-626). CRC Press. https://doi.org/10.1201/b11448

Paganetti, H. (2012). Range uncertainties in proton therapy and the role of Monte Carlo simulations. *Phys Med Biol*, *57*(11), R99-117. https://doi.org/10.1088/0031-9155/57/11/R99

Paganetti, H. (2014). Relative biological effectiveness (RBE) values for proton beam therapy. Variations as a function of biological endpoint, dose, and linear energy transfer. *Phys Med Biol*, *59*(22), R419-472. https://doi.org/10.1088/0031-9155/59/22/R419

Paganetti, H. (2018). Proton Relative Biological Effectiveness - Uncertainties and Opportunities. *Int J Part Ther*, *5*(1), 2-14. https://doi.org/10.14338/IJPT-18-00011.1

Paganetti, H, Blakely, E, Carabe-Fernandez, A, Carlson, D J, Das, I J, Dong, L, Grosshans, D, Held, K D, Mohan, R, Moiseenko, V, et al. (2019). Report of the AAPM TG-256 on the relative biological effectiveness of proton beams in radiation therapy. *Med Phys*, *46*(3), e53-e78. https://doi.org/10.1002/mp.13390

Paganetti, H, & Goitein, M. (2000). Radiobiological significance of beamline dependent proton energy distributions in a spread-out Bragg peak. *Med Phys*, *27*(5), 1119-1126. https://doi.org/10.1118/1.598977

Paganetti, H, Jiang, H, Lee, S Y, & Kooy, H M. (2004). Accurate Monte Carlo simulations for nozzle design, commissioning and quality assurance for a proton radiation therapy facility. *Med Phys*, *31*(7), 2107-2118. https://doi.org/10.1118/1.1762792

Paganetti, H, Jiang, H, Parodi, K, Slopsema, R, & Engelsman, M. (2008). Clinical implementation of full Monte Carlo dose calculation in proton beam therapy. *Phys Med Biol*, *53*(17), 4825-4853. https://doi.org/10.1088/0031-9155/53/17/023

Parodi, K, Mairani, A, Brons, S, Hasch, B G, Sommerer, F, Naumann, J, Jakel, O, Haberer, T, & Debus, J. (2012). Monte Carlo simulations to support start-up and treatment planning of scanned proton and carbon ion therapy at a synchrotron-based facility. *Phys Med Biol*, *57*(12), 3759-3784. https://doi.org/10.1088/0031-9155/57/12/3759

Parodi, K, Paganetti, H, Cascio, E, Flanz, J B, Bonab, A A, Alpert, N M, Lohmann, K, & Bortfeld, T. (2007). PET/CT imaging for treatment verification after proton therapy: a study with plastic phantoms and metallic implants. *Med Phys*, *34*(2), 419-435. https://doi.org/10.1118/1.2401042

Patrignani, C, Agashe, K, Aielli, G, Amsler, C, Antonelli, M, Asner, D M, Baer, H, Banerjee, S, Barnett, R M, Basaglia, T, et al. (2016). Review of Particle Physics. *Chinese Phys C*, *40*(10), 100001. https://doi.org/10.1088/1674-1137/40/10/100001

Pedersen, J, Petersen, J B B, Stokkevåg, C H, Ytre-Hauge, K S, Flampouri, S, Li, Z, Mendenhall, N, & Muren, L P. (2017). Biological dose and complication probabilities for the rectum and bladder based on linear energy transfer distributions in spot scanning proton therapy of prostate cancer. *Acta Oncol*, *56*(11), 1413-1419. https://doi.org/10.1080/0284186X.2017.1373198

Peeler, C R, Mirkovic, D, Titt, U, Blanchard, P, Gunther, J R, Mahajan, A, Mohan, R, & Grosshans, D R. (2016). Clinical evidence of variable proton biological effectiveness in pediatric patients treated for ependymoma. *Radiother Oncol*, *121*(3), 395-401. https://doi.org/10.1016/j.radonc.2016.11.001

Perl, J, Shin, J, Schumann, J, Faddegon, B, & Paganetti, H. (2012). TOPAS: an innovative proton Monte Carlo platform for research and clinical applications. *Med Phys*, *39*(11), 6818-6837. https://doi.org/10.1118/1.4758060

Petti, P L. (1996). Evaluation of a pencil-beam dose calculation technique for charged particle radiotherapy. *Int J Radiat Oncol Biol Phys*, *35*(5), 1049-1057. https://doi.org/10.1016/0360-3016(96)00233-7

Prusator, M, Ahmad, S, & Chen, Y. (2017). TOPAS Simulation of the Mevion S250 compact proton therapy unit. *J Appl Clin Med Phys*, *18*(3), 88-95. https://doi.org/10.1002/acm2.12077

PTCOG. (2021a). *Particle therapy facilities in clinical operation*. Retrieved 12.05.2020 from https://www.ptcog.ch/index.php/facilities-in-operation

PTCOG. (2021b). *Patient statistics*. Retrieved 12.05.2020 from https://www.ptcog.ch/index.php/patient-statistics

Ramos-Mendez, J, Perl, J, Faddegon, B, Schumann, J, & Paganetti, H. (2013). Geometrical splitting technique to improve the computational efficiency in Monte Carlo calculations for proton therapy. *Med Phys*, *40*(4), 041718. https://doi.org/10.1118/1.4795343

Ruddon, R W. (2007). *Cancer biology* (4th ed.). Oxford University Press.

Röntgen, W C. (1895). Ueber eine neue Art von Strahlen. *Sitzungsberichte der Physikalisch-medizinischen Gesellschaft zu Wuerzburg*, *29*, 132-141.

Rørvik, E, Fjæra, L F, Dahle, T J, Dale, J E, Engeseth, G M, Stokkevåg, C H, Thornqvist, S, & Ytre-Hauge, K S. (2018). Exploration and application of phenomenological RBE models for proton therapy.

Phys Med Biol, *63*(18), 185013. https://doi.org/10.1088/1361-6560/aad9db

Rørvik, E, Thornqvist, S, Stokkevåg, C H, Dahle, T J, Fjæra, L F, & Ytre-Hauge, K S. (2017). A phenomenological biological dose model for proton therapy based on linear energy transfer spectra. *Med Phys*, *44*(6), 2586-2594. https://doi.org/10.1002/mp.12216

Sanchez-Parcerisa, D, Cortes-Giraldo, M A, Dolney, D, Kondrla, M, Fager, M, & Carabe, A. (2016). Analytical calculation of proton linear energy transfer in voxelized geometries including secondary protons. *Phys Med Biol*, *61*(4), 1705-1721. https://doi.org/10.1088/0031-9155/61/4/1705

Sayah, R, Donadille, L, Aube, A, Herault, J, Delacroix, S, De Marzi, L, Stichelbaut, F, & Clairand, I. (2013). Monte Carlo simulation of a proton therapy beamline for intracranial treatments. *Radioprotection*, *48*(3), 317-339. https://doi.org/10.1051/radiopro/2012054

Schippers, J M. (2012). Beam Delivery Systems for Particle Radiation Therapy: Current Status and Recent Developments. *Reviews of Accelerator Science and Technology*, *02*(01), 179-200. https://doi.org/10.1142/s1793626809000211

Schippers, J M. (2015). Proton Beam Production and Dose Delivery Techniques. In I J Das & H Paganetti (Eds.), *Principles and Practice of Proton Beam Therapy* (1st ed., pp. 129-163). Medical Physics Publishing, Inc.

Schneider, U, Pedroni, E, & Lomax, A. (1996). The calibration of CT Hounsfield units for radiotherapy treatment planning. *Phys Med Biol*, *41*(1), 111-124. https://doi.org/10.1088/0031-9155/41/1/009

Schneider, W, Bortfeld, T, & Schlegel, W. (2000). Correlation between CT numbers and tissue parameters needed for Monte Carlo simulations of clinical dose distributions. *Phys Med Biol*, *45*(2), 459-478. https://doi.org/10.1088/0031-9155/45/2/314

Scholz, M, Kellerer, A M, Kraft-Weyrather, W, & Kraft, G. (1997). Computation of cell survival in heavy ion beams for therapy. The model and its approximation. *Radiat Environ Biophys*, *36*(1), 59-66. https://doi.org/10.1007/s004110050055

Schuemann, J, Giantsoudi, D, Grassberger, C, Moteabbed, M, Min, C H, & Paganetti, H. (2015). Assessing the Clinical Impact of Approximations in Analytical Dose Calculations for Proton

Therapy. *Int J Radiat Oncol Biol Phys*, *92*(5), 1157-1164. https://doi.org/10.1016/j.ijrobp.2015.04.006

Sethi, R V, Giantsoudi, D, Raiford, M, Malhi, I, Niemierko, A, Rapalino, O, Caruso, P, Yock, T I, Tarbell, N J, Paganetti, H, et al. (2014). Patterns of failure after proton therapy in medulloblastoma; linear energy transfer distributions and relative biological effectiveness associations for relapses. *Int J Radiat Oncol Biol Phys*, *88*(3), 655-663. https://doi.org/10.1016/j.ijrobp.2013.11.239

Shin, D, Yoon, M, Kwak, J, Shin, J, Lee, S B, Park, S Y, Park, S, Kim, D Y, & Cho, K H. (2009). Secondary neutron doses for several beam configurations for proton therapy. *Int J Radiat Oncol Biol Phys*, *74*(1), 260-265. https://doi.org/10.1016/j.ijrobp.2008.10.090

Shin, W G, Testa, M, Kim, H S, Jeong, J H, Lee, S B, Kim, Y J, & Min, C H. (2017). Independent dose verification system with Monte Carlo simulations using TOPAS for passive scattering proton therapy at the National Cancer Center in Korea. *Phys Med Biol*, *62*(19), 7598-7616. https://doi.org/10.1088/1361-6560/aa8663

Slopsema, R. (2011). Beam Delivery Using Passive Scattering. In H Paganetti (Ed.), *Proton Therapy Physics* (1st ed., pp. 125-156). CRC Press. https://doi.org/10.1201/b11448

Standring, S. (2016). *Gray's anatomy: the anatomical basis of clinical practice* (S Standring, Ed. 41st ed.). Elsevier Ltd.

Steliarova-Foucher, E, Colombet, M, Ries, L A G, Moreno, F, Dolya, A, Bray, F, Hesseling, P, Shin, H Y, Stiller, C A, & contributors, I-. (2017). International incidence of childhood cancer, 2001-10: a population-based registry study. *Lancet Oncol*, *18*(6), 719-731. https://doi.org/10.1016/S1470-2045(17)30186-9

Sung, H, Ferlay, J, Siegel, R L, Laversanne, M, Soerjomataram, I, Jemal, A, & Bray, F. (2021). Global Cancer Statistics 2020: GLOBOCAN Estimates of Incidence and Mortality Worldwide for 36 Cancers in 185 Countries. *CA Cancer J Clin*, *71*(3), 209-249. https://doi.org/10.3322/caac.21660

Sørensen, B S. (2019). Commentary: RBE in proton therapy - where is the experimental in vivo data? *Acta Oncol*, *58*(10), 1337-1339. https://doi.org/10.1080/0284186X.2019.1669819

Sørensen, B S, Bassler, N, Nielsen, S, Horsman, M R, Grzanka, L, Spejlborg, H, Swakon, J, Olko, P, & Overgaard, J. (2017). Relative biological effectiveness (RBE) and distal edge effects of proton

radiation on early damage in vivo. *Acta Oncol*, *56*(11), 1387-1391. https://doi.org/10.1080/0284186X.2017.1351621

Sørensen, B S, Overgaard, J, & Bassler, N. (2011). In vitro RBE-LET dependence for multiple particle types. *Acta Oncol*, *50*(6), 757-762. https://doi.org/10.3109/0284186X.2011.582518

Saager, M, Peschke, P, Brons, S, Debus, J, & Karger, C P. (2018). Determination of the proton RBE in the rat spinal cord: Is there an increase towards the end of the spread-out Bragg peak? *Radiother Oncol*, *128*(1), 115-120. https://doi.org/10.1016/j.radonc.2018.03.002

Tepper, J, Verhey, L, Goitein, M, Suit, H D, Phil, D, & Koehler, A M. (1977). In vivo determinations of RBE in a high energy modulated proton beam using normal tissue reactions and fractionated dose schedules. *Int J Radiat Oncol Biol Phys*, *2*(11-12), 1115-1122. https://doi.org/10.1016/0360-3016(77)90118-3

Thames, H D, & Suit, H D. (1986). Tumor radioresponsiveness versus fractionation sensitivity. *Int J Radiat Oncol Biol Phys*, *12*(4), 687-691. https://doi.org/10.1016/0360-3016(86)90081-7

Thariat, J, Hannoun-Levi, J M, Sun Myint, A, Vuong, T, & Gerard, J P. (2013). Past, present, and future of radiotherapy for the benefit of patients. *Nat Rev Clin Oncol*, *10*(1), 52-60. https://doi.org/10.1038/nrclinonc.2012.203

The Global Cancer Observatory. (2020). *Cancer Today*. Retrieved 22.05.2021 from https://gco.iarc.fr/today/home

Uh, J, Merchant, T E, Li, Y, Feng, T, Gajjar, A, Ogg, R J, & Hua, C. (2013). Differences in brainstem fiber tract response to radiation: a longitudinal diffusion tensor imaging study. *Int J Radiat Oncol Biol Phys*, *86*(2), 292-297. https://doi.org/10.1016/j.ijrobp.2013.01.028

Underwood, T S A, Grassberger, C, Bass, R, MacDonald, S M, Meyersohn, N M, Yeap, B Y, Jimenez, R B, & Paganetti, H. (2018). Asymptomatic Late-phase Radiographic Changes Among Chest-Wall Patients Are Associated With a Proton RBE Exceeding 1.1. *Int J Radiat Oncol Biol Phys*, *101*(4), 809-819. https://doi.org/10.1016/j.ijrobp.2018.03.037

Unkelbach, J, Alber, M, Bangert, M, Bokrantz, R, Chan, T C Y, Deasy, J O, Fredriksson, A, Gorissen, B L, van Herk, M, Liu, W, et al. (2018). Robust radiotherapy planning. *Phys Med Biol*, *63*(22), 22TR02. https://doi.org/10.1088/1361-6560/aae659

Unkelbach, J, Botas, P, Giantsoudi, D, Gorissen, B L, & Paganetti, H. (2016). Reoptimization of Intensity Modulated Proton Therapy Plans Based on Linear Energy Transfer. *Int J Radiat Oncol Biol Phys*, *96*(5), 1097-1106. https://doi.org/10.1016/j.ijrobp.2016.08.038

Urano, M, Goitein, M, Verhey, L, Mendiondo, O, Suit, H D, & Koehler, A. (1980). Relative biological effectiveness of a high energy modulated proton beam using a spontaneous murine tumor In vivo. *Int J Radiat Oncol Biol Phys*, *6*(9), 1187-1193. https://doi.org/10.1016/0360-3016(80)90172-8

van Leeuwen, C M, Oei, A L, Crezee, J, Bel, A, Franken, N A P, Stalpers, L J A, & Kok, H P. (2018). The alfa and beta of tumours: a review of parameters of the linear-quadratic model, derived from clinical radiotherapy studies. *Radiat Oncol*, *13*(1), 96. https://doi.org/10.1186/s13014-018-1040-z

Verburg, J M, Grassberger, C, Dowdell, S, Schuemann, J, Seco, J, & Paganetti, H. (2016). Automated Monte Carlo Simulation of Proton Therapy Treatment Plans. *Technol Cancer Res Treat*, *15*(6), NP35-NP46. https://doi.org/10.1177/1533034615614139

Vlachoudis, V. (2009, May 3-7). FLAIR: A Powerful But User Friendly Graphical Interface For FLUKA. International Conference on Mathematics, Computational Methods & Reactor Physics (M&C 2009), Saratoga Springs, New York. http://www.fluka.org/FLUKA/flair/Flair_MC2009.pdf

Wang, C C, McNamara, A L, Shin, J, Schuemann, J, Grassberger, C, Taghian, A G, Jimenez, R B, MacDonald, S M, & Paganetti, H. (2020). End-of-Range Radiobiological Effect on Rib Fractures in Patients Receiving Proton Therapy for Breast Cancer. *Int J Radiat Oncol Biol Phys*, *107*(3), 449-454. https://doi.org/10.1016/j.ijrobp.2020.03.012

Wedenberg, M, Lind, B K, & Hardemark, B. (2013). A model for the relative biological effectiveness of protons: the tissue specific parameter alpha/beta of photons is a predictor for the sensitivity to LET changes. *Acta Oncol*, *52*(3), 580-588. https://doi.org/10.3109/0284186X.2012.705892

Wilkens, J J, & Oelfke, U. (2003). Analytical linear energy transfer calculations for proton therapy. *Med Phys*, *30*(5), 806-815. https://doi.org/10.1118/1.1567852

Wilkens, J J, & Oelfke, U. (2004a). A phenomenological model for the relative biological effectiveness in therapeutic proton beams. *Phys Med Biol*, *49*(13), 2811-2825. https://doi.org/10.1088/0031-9155/49/13/004

Wilkens, J J, & Oelfke, U. (2004b). Three-dimensional LET calculations for treatment planning of proton therapy. *Z Med Phys*, *14*(1), 41-46. https://doi.org/10.1078/0939-3889-00191

Wilson, R R. (1946). Radiological use of fast protons. *Radiology*, *47*(5), 487-491. https://doi.org/10.1148/47.5.487

Yepes, P, Adair, A, Frank, S J, Grosshans, D R, Liao, Z, Liu, A, Mirkovic, D, Poenisch, F, Titt, U, Wang, Q, et al. (2019). Fixed- versus Variable-RBE Computations for Intensity Modulated Proton Therapy. *Adv Radiat Oncol*, *4*(1), 156-167. https://doi.org/10.1016/j.adro.2018.08.020

Yepes, P, Adair, A, Grosshans, D, Mirkovic, D, Poenisch, F, Titt, U, Wang, Q, & Mohan, R. (2018). Comparison of Monte Carlo and analytical dose computations for intensity modulated proton therapy. *Phys Med Biol*, *63*(4), 045003. https://doi.org/10.1088/1361-6560/aaa845

Ytre-Hauge, K S, Fjæra, L F, Rørvik, E, Dahle, T J, Dale, J E, Pilskog, S, & Stokkevåg, C H. (2020). Inter-patient variations in relative biological effectiveness for cranio-spinal irradiation with protons. *Sci Rep*, *10*(1), 6212. https://doi.org/10.1038/s41598-020-63164-8

Zhu, X R, Poenisch, F, Li, H, Zhang, X, Sahoo, N, & Gillin, M T. (2015). Field Shaping: Scanning Beam. In I J Das & H Paganetti (Eds.), *Principles and Practice of Proton Beam Therapy* (1st ed., pp. 209-228). Medical Physics Publishing, Inc.

Ödén, J, Eriksson, K, & Toma-Dasu, I. (2017). Inclusion of a variable RBE into proton and photon plan comparison for various fractionation schedules in prostate radiation therapy. *Med Phys*, *44*(3), 810-822. https://doi.org/10.1002/mp.12117

Ödén, J, Toma-Dasu, I, Witt Nystrom, P, Traneus, E, & Dasu, A. (2020). Spatial correlation of linear energy transfer and relative biological effectiveness with suspected treatment-related toxicities following proton therapy for intracranial tumors. *Med Phys*, *47*(2), 342-351. https://doi.org/10.1002/mp.13911

Graphic design: Communication Division, UiB / Print: Skipnes Kommunikasjon AS

uib.no

ISBN: 9788230854945 (print)
9788230866566 (PDF)